THE ASTROPHYSICAL JOURNAL, 293:102–119, 1985 June 1

HOT CORONAE AROUND EARLY-TYPE GALAXIES

W. FORMAN AND C. JONES
Harvard-Smithsonian Center for Astrophysics
AND
W. TUCKER
Harvard-Smithsonian Center for Astrophysics
Received 1984 September 7; accepted 1984 November 15

ABSTRACT

The analysis of the X-ray emission from a sample of 55 bright early-type galaxies shows that hot gaseous coronae are a common and perhaps ubiquitous feature of such systems. The X-ray emission can be explained most naturally as thermal bremsstrahlung from hot gas ($kT \approx 0.5$–1.5 keV) which may be accumulated from mass loss during normal stellar evolution. The presence of these coronae shows that matter (10^9–10^{10} $M_\odot$) previously thought to be expelled in a galactic wind is instead stored in a hot galactic corona which may be heated and powered by supernova explosions. Perhaps the single most important feature of these coronae is that they provide a unique tracer of the gravitational potential in the outer regions of bright early-type galaxies. In this paper we describe the X-ray properties of these coronae (gas mass, temperature, and extent) and discuss their implications for the presence of massive dark halos around individual early-type galaxies. We find total masses of early-type galaxies up to 5×10^{12} $M_\odot$. We estimate mass-to-light ratios for early-type galaxies and find values up to ~ 100 (in solar units), similar to those found for the larger dynamical systems of groups and clusters.

Subject headings: galaxies: structure — galaxies: X-rays

I. INTRODUCTION

To understand the formation of galaxies and larger scale structures, one must determine the distribution of both visible and invisible matter in individual galaxies. While extensive optical observations have provided information on galaxy kinematics (Illingworth 1977; Kormendy and Illingworth 1982; Davies *et al.* 1983; Dressler and Sandage 1983), as Caldwell (1984) has noted, "all of this work on E's has not answered either of two questions for even one galaxy: the radial distribution of matter as opposed to that of the light, and the large-scale geometric structure of the matter. To study the mass distribution in an E galaxy we would like to use test particles that are visibly distinct objects from the stars and contribute negligibly to the total galaxy mass." As is shown in the present paper, the extended X-ray–emitting gas observed around early-type galaxies provides a tool for addressing these questions.

Dynamical investigations of elliptical-dominated groups and rich clusters (predominantly early-type galaxies) suggest that only a small fraction of the total mass of the system is contained within the optically observable galaxies. However, the absence in general of a cool interstellar medium makes the study of the dynamical masses in individual early-type galaxies difficult with traditional optical and radio techniques which are so powerful in studying later type spiral galaxies (e.g., Rubin, Ford, and Thonnard 1978, 1980; Rubin, Burstein, and Thonnard 1980; Rubin *et al.* 1982; Burstein *et al.* 1982). The inability to determine the total masses of individual early-type galaxies at large radii has prevented the direct measurement of mass-to-light ratios outside the core which could then be compared to mass-to-light ratios for groups and clusters to test whether the large fraction of dark matter in these systems was once associated with galaxies. The analysis of the X-ray observations of the hot coronae presented here suggests that the mass-to-light ratios of early-type galaxies can be as large as ~ 100 (in solar units) and approach those of groups and clusters. Thus, since early-type galaxies are the primary constituents of rich clusters, much of the dark matter in groups and clusters may have been found initially in the galaxy halos.

The same X-ray observations which we use to map the mass distributions in early-type galaxies also provide information concerning the fate of gas lost from the present epoch stars during their evolution. The general absence of gas in elliptical and S0 galaxies was reviewed by Faber and Gallagher (1976, hereafter FG). They argued that mass loss from dying stars would produce sufficient mass to be observable in either H I (if the gas were cold), optical emission lines (if the gas were warm, $T \sim 10^4$ K), or forbidden emission lines (if the gas were hot, $T \sim 4 \times 10^6$ K). Dense clouds of neutral hydrogen or H_2 were found to be either physically unreasonable or readily observable, and initially cold hydrogen ($T \sim 2.7$ K) would be heated by collisions with clouds or shells of matter subsequently shed by stars. The difficulties of storing mass accumulated over time scales of 10^8–10^9 years from present epoch stellar populations are further aggravated if one tries to account for the mass shed over the entire life of the galaxy. As FG point out, the time-averaged mass loss rate over a galaxy's lifetime is 50 times higher than the present rate, since much larger amounts of mass were lost from younger, more massive stars at earlier epochs. The absence of detections of significant amounts of matter in any of the forms described above led FG to conclude that the mass shed by evolving and dying stars is most likely ejected in a wind like that proposed by Mathews and Baker (1971, hereafter MB). Hot winds from galaxies such as those modeled by MB are difficult to detect. Hot gas is continuously ejected from the galaxy, and thus gas densities are low. The resulting luminosities in soft X-rays are only 10^{36} ergs s^{-1} (MB) spread over a 10 kpc radius region and are effectively undetectable even in long *Einstein* observations. Thus, the dis-

covery that gaseous coronae with X-ray luminosities up to 10^6 times larger than that predicted by MB are a common property of early-type galaxies argues that these galaxies are sufficiently massive to bind their atmospheres and suppress a total wind.

In this paper we report on X-ray observations of early-type galaxies (elliptical, S0, and Sa) in a variety of environments including cluster outskirts and the field. None of the galaxies in our sample lie at the centers of rich clusters, where extensive diffuse X-ray emission is usually seen. Previous works (Forman *et al.* 1979; Bechtold *et al.* 1983; Biermann and Kronberg 1983; Nulsen, Stewart, and Fabian 1984) reported hot coronae around galaxies but did not resolve whether the phenomenon was universal or was associated with a certain type of galaxy or found in a particular environment (e.g., groups and clusters). The more extensive material presented in this paper shows that gaseous coronae are a common feature of bright ($M_B \lesssim -19$) early-type galaxies. We observe extended coronae around Sa, lenticular, and elliptical galaxies. These coronae have X-ray luminosities in the range 10^{39}–10^{42} ergs s^{-1} (from 0.5 to 4.5 keV). When the angular resolution of our observations is sufficient, the coronae are resolved and are observed to have extents as large as ~ 100 kpc, well beyond the Holmberg radius of the galaxy. We have determined integrated temperatures of ~ 1 keV (with a range of 0.5–1.5 keV). The inferred gas masses of these hot coronae are 5×10^8 to $5 \times 10^{10}\ M_\odot$ and thus represent only a very small fraction of the total galaxy mass and a small fraction of the total gas liberated by galaxies, given the large mass loss rates expected at early epochs. Norman and Silk (1979) suggested that sufficiently massive galaxies could maintain hot coronae at all stages of their evolution, and they argued in favor of the existence of hot coronae with parameters similar to those determined from the X-ray observations. The X-ray luminosity of the corona is correlated with the absolute blue magnitude of the galaxy and thus with the stellar galaxy mass. Finally, we suggest that the energy liberated by supernovae is sufficient to heat and continuously power the coronae through the conversion of kinetic into thermal energy. Thus, more massive galaxies can maintain more luminous coronae.

Not only is the gas produced by the evolution of stellar systems detectable in early-type galaxies, but this gas can be used to probe the mass distributions of these galaxies (which, as noted above, generally lack the radio and optically emitting material used to study later type galaxies). The mere presence of hot coronae, i.e., the suppression of a wind, in itself argues that early-type galaxies have massive halos. Optical observations which determine the structure and velocity dispersion of the galaxy core yield mass-to-light ratios of 5–10 (e.g., Faber and Gallagher 1979). The mass-to-light ratios reported in this paper are determined over larger regions and exceed the core values by up to a factor of 10. Quantitatively, using the hot coronae as probes, we estimate the total galaxy masses to be $\sim(1\text{–}5) \times 10^{12}\ M_\odot$.

II. OBSERVATIONS AND ANALYSIS

a) The Galaxy Sample

We have selected a sample of 55 early-type galaxies which were observed with the *Einstein Observatory* imaging detectors. For 39 of these galaxies (those targeted in the Center for Astrophysics [CfA] program and those in the *Einstein* Data Bank), we have carried out an analysis which is described below. Stanger and Schwarz (1984) have studied a subset of these galaxies, and their fluxes are in agreement with ours. X-ray fluxes for the remaining galaxies have been taken from the work of Long and Van Speybroeck (1983) or Nulsen, Stewart, and Fabian (1984). The galaxy sample spans a wide range in absolute magnitude (-23.1 to -18.6) and includes representatives of all early-type galaxies (E, S0, and Sa).

Each galaxy included in this survey is listed in Table 1 along with its absolute blue magnitude, usually from the *Revised Shapley-Ames Catalog* (Sandage and Tammann 1981), and a description of the galaxy's environment. Twenty of the galaxies in this sample lie in the Virgo Cluster. Two (NGC 4374 and NGC 4406) are in the Virgo core, where their coronae are affected by M87's halo (Forman *et al.* 1979; Fabian, Schwarz, and Forman 1980). The remaining galaxies are found primarily in low velocity dispersion groups ($v^2 \sim 200$ km s^{-1}) (Huchra and Geller 1982; Geller and Huchra 1983). For galaxies in these groups as well as those outside the Virgo core, with the exception of NGC 3585 (see Fig. 1), no extended emission is detected other than that associated with the galaxy.

b) X-Ray Analysis

Our analysis for the early-type galaxies includes four steps. These are (1) the computation of X-ray fluxes for each galaxy, (2) the production of isointensity contour plots for galaxies with detected X-ray emission, (3) the determination of the radial surface brightness distribution so that extent and parameters such as core radius and gas mass can be determined, and (4) the measurement of the X-ray energy spectrum. We now describe each step of the analysis in some detail.

To determine the X-ray flux from each galaxy, we used the *Einstein* image-processing system to measure the number of photons from a region centered on the galaxy and the number of background photons obtained in a region $\geq 8'$ from the galaxy (but still within the same image). In order to measure the total flux from each galaxy, consecutively larger regions around the galaxy were measured until a size was reached in which there was no increase in the net number of photons (after subtracting the background contribution). For the *Einstein* imaging proportional counter (IPC) observations, we used the energy range from 0.5 to 4.5 keV.[1] For the *Einstein* high-resolution imager (HRI), all data are obtained in the 0.1–4.5 keV energy band. The measured X-ray fluxes are converted to X-ray luminosities using the galaxy (or group) velocities (taken when available from Sandage and Tammann 1981) listed in Table 1, with an H_0 of 50 km s^{-1} Mpc^{-1}. For those galaxies in the Long and Van Speybroeck (1983) sample which are either CfA or Data Bank observations, we have recomputed the X-ray fluxes. Although we measured the total X-ray flux, while Long and Van Speybroeck measured that within a given optical isophotal radius, the measured X-ray counting rates generally agree. Exceptions include galaxies with very extended X-ray emission (e.g., NGC 4636) or those with a nearby serendipitous source. Differences in X-ray luminosities therefore are attributable primarily to different conversions of counting rate to flux and different assumed galaxy distances.

For each galaxy from which X-ray emission was detected, we generated isointensity contours of the X-ray emission which we

[1] Revisions to the IPC calibration were derived as part of the *Einstein* Revision 1 processing effort. These revisions have resulted in a modified correspondence between pulse-height channel and energy. Throughout this paper we have used the Revision 1 calibration.

TABLE 1

DESCRIPTION OF GALAXY SAMPLE

Galaxy (Type)	V_0[a]	M_B[b]	L_x (ergs s^{-1})	Group or Cluster Environment[c]
NGC 315 (E/S0)	4910DV	−22.86	$7.99 \pm 0.42 \times 10^{41}$	GH 8
NGC 524 (S0/Sa)	2566	−21.90	$7.59 \pm 1.31 \times 10^{40}$	GH 13
NGC 720 (E5)	1771	−21.60	1.3×10^{41}[d]	Cetus II group (DV 33, HG 45)
NGC 936 (SB0/SBa)	1512	−21.21	$<8.4 \times 10^{40}$[d]	Cetus I group (DV 15, GH 28)
NGC 1172 (S0)	1566	−19.48	$<9.3 \times 10^{39}$[e]	
NGC 1316 (For A Sa pec)	1486F	−23.08	$8.89 \pm 0.77 \times 10^{40}$	DV 53, HG 17
NGC 1332 (S0)	1455	−21.03	$5.33 \pm 0.40 \times 10^{40}$[f]	HG 32
NGC 1380 (S0/Sa)	1486F	−21.30	4.6×10^{40}[d]	Fornax (DV 53, HG 17)
NGC 1395 (E2)	1664	−21.43	$9.16 \pm 0.51 \times 10^{40}$	HG 32
NGC 1533 (SB0/SBa)	559	−18.59	$1.86 \pm 0.34 \times 10^{39}$[f]	HG 3
NGC 1574 (SB0)	701	−19.60	$<1.3 \times 10^{40}$[d]	HG 3
NGC 1600 (E4)	4734	−22.87	$6.56 \pm 1.3 \times 10^{41}$	
NGC 2300 (E3)	2190	−21.22	$1.14 \pm 0.20 \times 10^{41}$	HG 92
NGC 2563 (S0; E)	4542DV	−21.6	$3.60 \pm 0.40 \times 10^{41}$	Cancer
NGC 2685 (S0 pec)	1001	−19.65	$5.23 \pm 2.87 \times 10^{39}$	HG 80
NGC 2859 (RSB0)	1590	−20.76	$<1.1 \times 10^{40}$	GH 43
NGC 2974 (E4)	1814	−21.12	$3.50 \pm 0.70 \times 10^{40}$[e]	
NGC 3258 (E1)	2553	−21.06	$1.59 \pm 0.30 \times 10^{41}$	HG 18
NGC 3377 (E6)	591	−19.26	$<3.5 \times 10^{39}$[d]	Leo (DV 11, HG 56, GH 68)
NGC 3489 (S0/Sa)	532	−19.00	$<3.5 \times 10^{39}$[d]	GH 68
NGC 3593 (Sa pec)	493	−19.19	3.3×10^{39}[d]	Leo (DV 9, HG 56)
NGC 3585 (E7/S0)	1212	−21.11	$8.00 \pm 2.00 \times 10^{39}$[f]	
N3718 (Sa pec)	1082	−21.24	$<2.60 \times 10^{40}$	Ursa Minor I (DV 34, HG 60)
NGC 3818 (E5)	1286	−19.26	$<2.6 \times 10^{40}$[d]	NGC 3672 group (DV 23)
NGC 3923 (E4/S0)	1509	−21.61	6.5×10^{40}[d]	NGC 3923 group (DV 44, HG 28)
NGC 4251 (S0)	971	−19.82	$2.28 \pm 1.26 \times 10^{39}$[f]	HG 60
NGC 4365 (E3)	1026V	−21.10	$1.24 \pm 0.15 \times 10^{40}$	Virgo, HG 41, GH 106
NGC 4374 (M84 E1)	1026V	−21.47	$3.92 \pm 0.28 \times 10^{40}$	Virgo, HG 41, GH 106
NGC 4382 (M85 S0 pec)	1026V	−21.60	$1.81 \pm 0.09 \times 10^{40}$	Virgo, HG 41, GH 106
NGC 4406 (M86 S0/E3)	1026V	−21.68	$2.42 \pm 0.07 \times 10^{41}$	Virgo, HG 41, GH 106
NGC 4459 (S0)	1026V	−20.21	$8.36 \pm 2.35 \times 10^{39}$	Virgo, HG 41, GH 106
NGC 4472 (M49 E1/S0)	1026V	−22.38	$3.30 \pm 0.08 \times 10^{41}$	Virgo, DV 19, HG 41, GH 106
NGC 4473 (E5)	1026V	−20.63	$7.23 \pm 2.61 \times 10^{39}$	Virgo, HG 41, GH 106
NGC 4477 (SB0/SBa)	1026V	−20.46	$8.79 \pm 2.67 \times 10^{39}$	Virgo, HG 41, GH 106
NGC 4550 (E7/S0)	1026V	−19.37	$<5.53 \times 10^{39}$	Virgo, HG 41, GH 106
NGC 4552 (M89 S0)	1026V	−20.9	$2.97 \pm 0.25 \times 10^{40}$	Virgo, HG 41, GH 106
NGC 4564 (E6)	1026V	−19.83	$<4.36 \times 10^{39}$	Virgo, HG 41, GH 106
NGC 4594 (Sa)	873	−22.81	$5.54 \pm 0.31 \times 10^{40}$	Virgo, HG 41
NGC 4636 (E0/S0)	821	−20.58	$1.78 \pm 0.10 \times 10^{41}$	Virgo, DV 26, HG 41, GH 106
NGC 4638 (S0)	1026V	−19.65	2.5×10^{39}	Virgo, HG 41, GH 106
NGC 4643 (SB0/SBa)	1271	−20.48	$<5.9 \times 10^{40}$[d]	Virgo, HG 41, GH 106
NGC 4649 (M60 S0)	1026V	−21.87	$1.56 \pm 0.06 \times 10^{41}$[f]	Virgo, DV 19, HG 41, GH 106
NGC 4665 (SB0/SBa)	629	−19.07	$1.94 \pm 0.43 \times 10^{39}$	Virgo, HG 41, GH 106
NGC 4697 (E6)	1033	−21.47	$1.20 \pm 0.13 \times 10^{40}$	Virgo, DV 20, HG 41
NGC 4698 (Sa)	1147VR	−20.55	$4.15 \pm 1.80 \times 10^{39}$	Virgo, HG 41, GH 106
NGC 4753 (S0 pec)	1117	−20.90	$9.30 \pm 1.38 \times 10^{39}$[f]	Virgo, HG 41
NGC 5101 (SBa)	1611	−21.06	$<3.09 \times 10^{40}$	
NGC 5102 (S0)	255C	−18.73	$<9.7 \times 10^{38}$[f]	HG 19
NGC 5128 (S0 + S pec Cen A)	255C	−22.6C	$5.6 \pm 0.11 \times 10^{39}$[g]	NGC 5128 group (DV 4, HG 19)
NGC 5532	7106DV		5.6×10^{41}[d]	
NGC 5866 (M102 S0)	824	−20.22	$6.38 \pm 2.12 \times 10^{39}$	NGC 5866 group (DV 3, HG 78, GH 152)
NGC 5898 (S0)	2098	−20.70	3.2×10^{40}[d]	
NGC 6876 (E3)	3791	−21.95	$3.22 \pm 0.28 \times 10^{41}$[e]	DV 38
IC 1459 (E4)	1638	−21.61	$4.90 \pm 0.55 \times 10^{40}$	HG 15
IC 4296 (E0)	3378	−22.72	$2.17 \pm 0.12 \times 10^{41}$	

[a] Origin of recession velocity is predominantly from Sandage and Tammann 1981. V, VR, F, and C refer to the mean velocities of groups of galaxies as given by Sandage and Tammann 1981 (V = Virgo core, VR = Virgo, outside core, F = Fornax, C = NGC 5128 group). Recession velocities from de Vaucouleurs, de Vaucouleurs, and Corwin 1976 are marked DV.

[b] Absolute blue magnitudes of Sandage and Tammann 1981 were converted to luminosities using an absolute magnitude for the Sun of 5.48.

[c] Origin of environment classification; DV = de Vaucouleurs 1975, Virgo = Huchra and Geller 1982 and Geller and Huchra 1983, HG = Huchra and Geller 1982, GH = Geller and Huchra 1983.

[d] Luminosities determined by Long and Van Speybroeck 1983 but corrected for V_0 in col. (2) and for flux normalization based on a 1 keV source temperature.

[e] Luminosities determined by Nulsen, Stewart, and Fabian 1984 but corrected for V_0 in col. (2).

[f] Values agree with those of Stanger and Schwarz 1984, corrected to the value of V_0 given in col. (2).

[g] See text for a discussion of the X-ray luminosity.

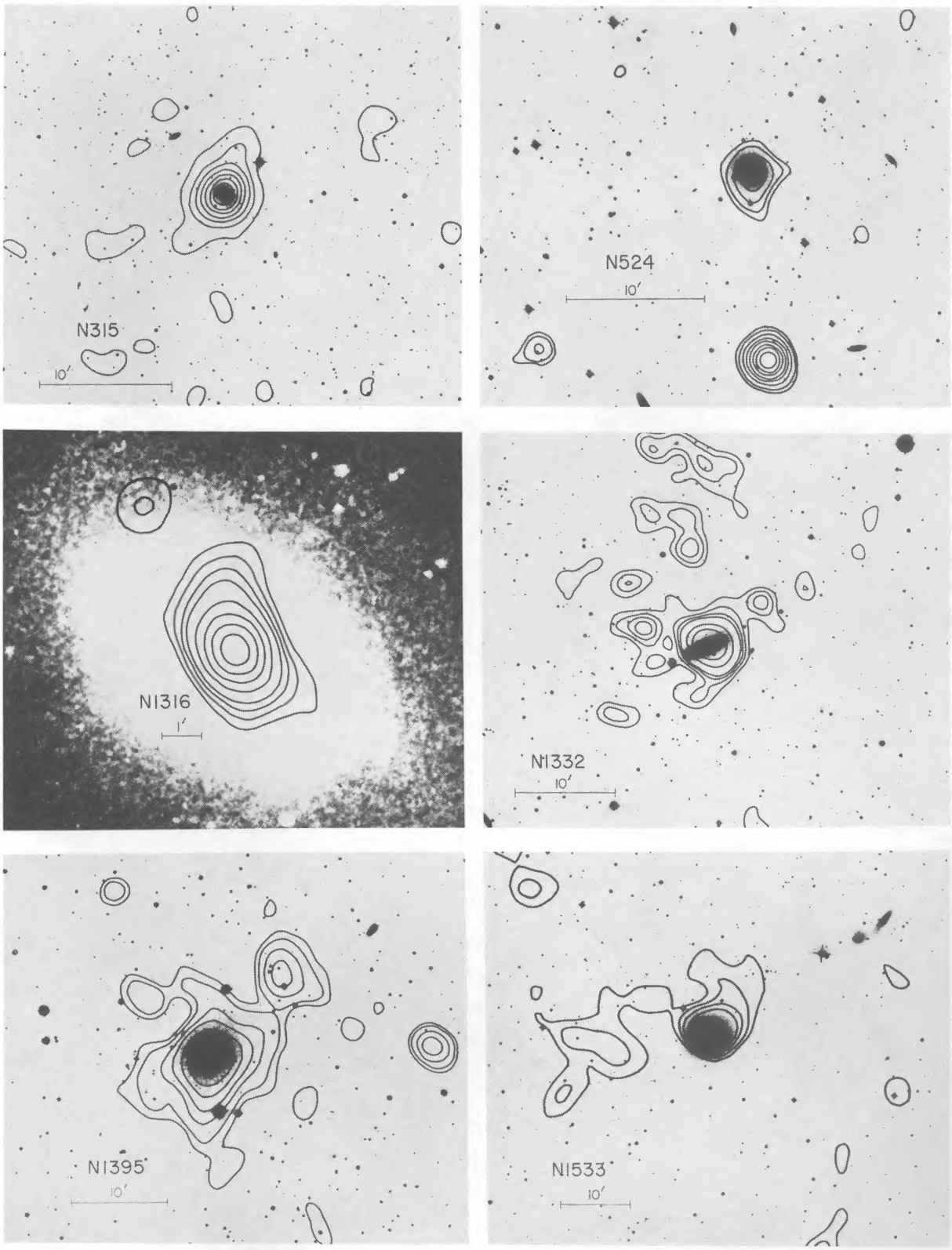

FIG. 1.—Isointensity plots of the X-ray emission are shown for 31 early-type galaxies. For the IPC observations, the emission is smoothed with a Gaussian of 45″, while for the HRI contour maps (NGC 1316 and NGC 4649) the X-ray emission is smoothed with a 20″ Gaussian. (*a*) N315: contour levels are 1.45E−4, 3.92E−4, 7.10E−4, 1.09E−3, 1.52E−3, 2.00E−3, 2.52E−3, and 3.09E−3 counts s^{-1} $arcmin^{-2}$ for significance levels 3 σ, 7 σ, 11 σ, 15 σ, 19 σ, 23 σ, 27 σ, and 31 σ. N1316: (HRI) contour levels are 1.42E−3, 1.92E−3, 2.45E−3, 2.97E−3, 4.10E−3, 5.22E−3, 6.44E−3, and 7.67E−3 counts s^{-1} $arcmin^{-2}$ for significance level 3 σ, 4 σ, 5 σ, 6 σ, 8 σ, 10 σ, 12 σ, and 14 σ. N1332: contour levels are 1.77E−4, 2.45E−4, 3.19E−4, 3.98E−3, 7.67E−4, 1.20E−3, and 1.97E−3 counts s^{-1} $arcmin^{-2}$ for significance levels 3 σ, 4 σ, 5 σ, 6 σ, 10 σ, 14 σ, and 20 σ. N1395: contour levels are 2.85E−4, 3.65E−4, 5.41E−4, 6.33E−4, 8.30E−4, 1.28E−3, and 1.78E−3 counts s^{-1} $arcmin^{-2}$ for significance levels 3 σ, 5 σ, 7 σ, 8 σ, 10 σ, 14 σ, and 18 σ. N1533: contour levels are 1.98E−4, 1.74E−4, 3.51E−4, 4.37E−4, 6.20E−4, and 8.14E−4 counts s^{-1} $arcmin^{-2}$ for significance levels 3 σ, 4 σ, 5 σ, 6 σ, 8 σ, and 10 σ.

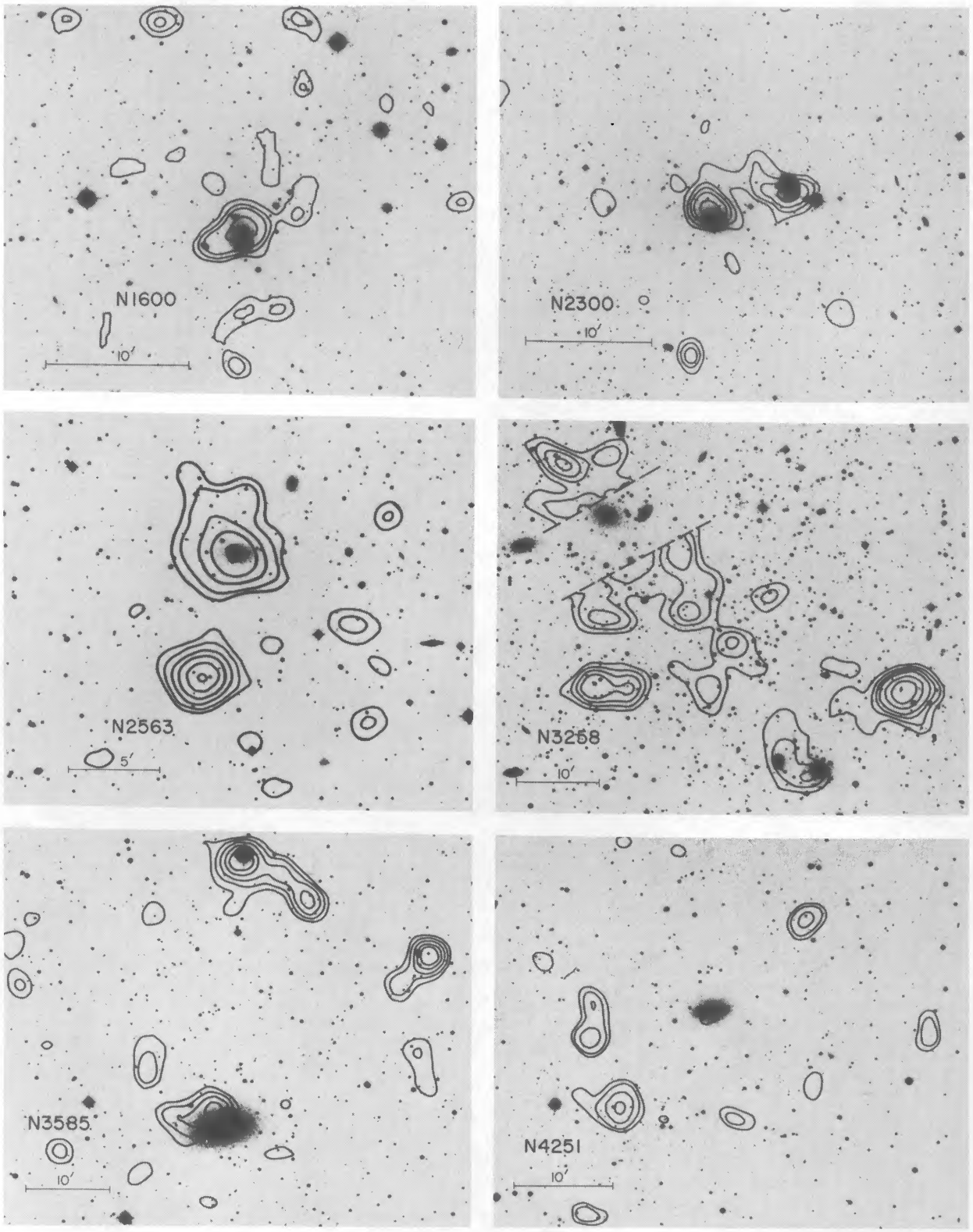

FIG. 1*b*.—N1600: contour levels are 6.75E−4, 9.82E−4, 1.32E−3, and 2.17E−3 counts s^{-1} $arcmin^{-2}$ for significance levels 3 σ, 4 σ, 5 σ, and 7 σ. N2300: contour levels are 5.60E−4, 8.04E−4, 1.06E−3, 1.39E−3, and 2.07E−3 counts s^{-1} $arcmin^{-2}$ for significance levels 3 σ, 4 σ, 5 σ, 6 σ, and 8 σ. N2563: contour levels are 2.63E−4, 3.67E−4, 5.89E−4, 8.47E−4, 1.27E−3 and 1.74E−3 counts s^{-1} $arcmin^{-2}$ for significance levels 3 σ, 4 σ, 6 σ, 8 σ, 11 σ, and 14 σ. N3258: contour levels are 6.85E−4, 9.57E−4, 1.26E−3, 1.60E−3, 2.32E−3, and 3.15E−3 counts s^{-1} $arcmin^{-2}$ for significance levels 3 σ, 4 σ, 5 σ, 6 σ, 8 σ, and 10 σ. To the northeast of N3258 is cluster X-ray emission partially obscured by the IPC window support ("ribs"). N3585: contour levels are 2.19E−4, 3.05E−4, 3.99E−4, 5.00E−4, and 6.02E−4 counts s^{-1} $arcmin^{-2}$ for significance levels 3 σ, 4 σ, 5 σ, 6 σ, and 7 σ. N4251: contour levels are 1.98E−4, 2.80E−4, 4.44E−4, and 6.31E−4 counts s^{-1} $arcmin^{-2}$ for significance levels 3 σ, 4 σ, 6 σ, and 8 σ.

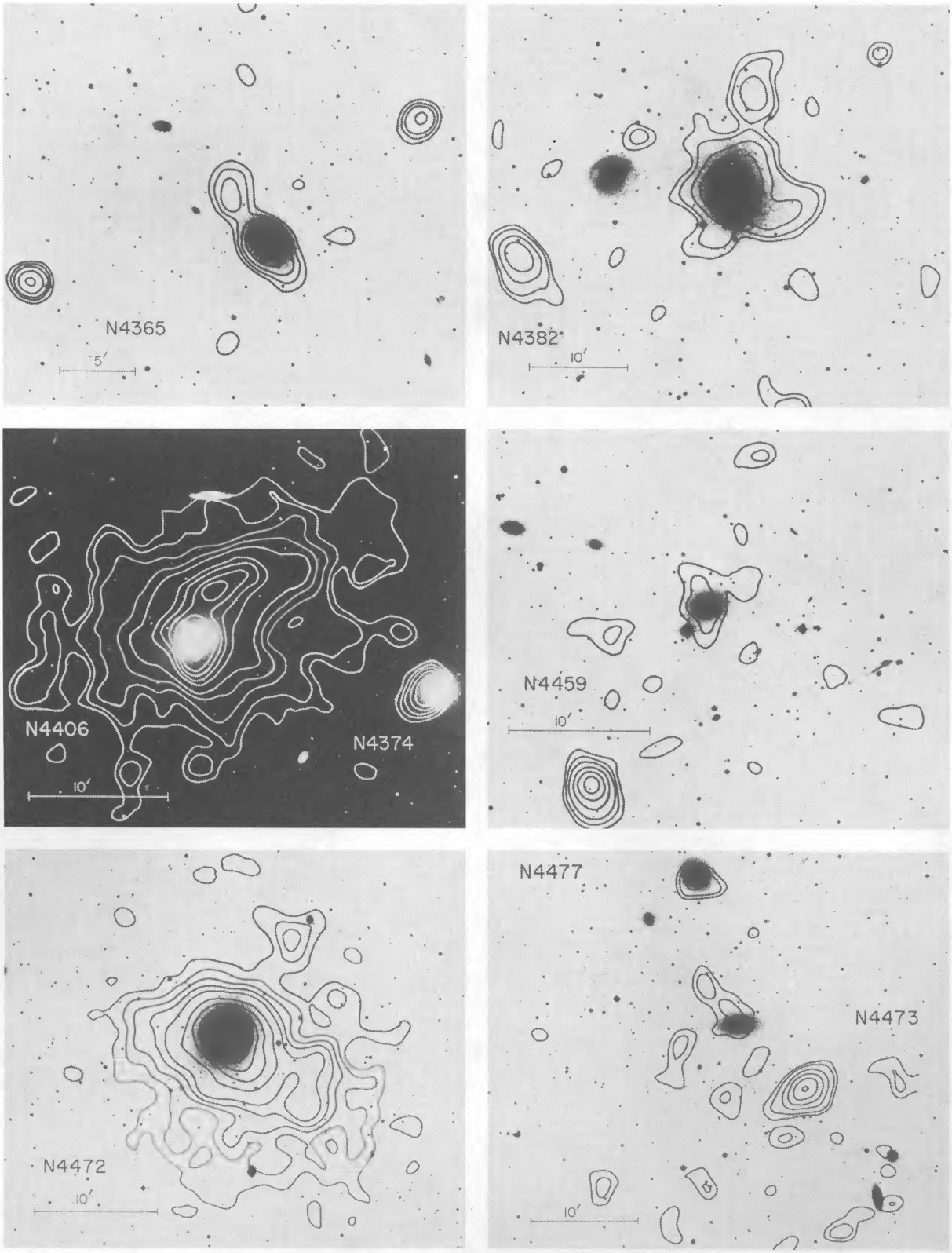

FIG. 1c.—N4365: contour levels are 2.24E−4, 3.11E−4, 4.04E−4, 6.05E−4, 8.28E−4, and 1.07E−3 counts s^{-1} $arcmin^{-2}$ for significance levels 3 σ, 4 σ, 5 σ, 7 σ, 9 σ, and 11 σ. N4382: contour levels are 1.47E−4, 2.02E−4, 3.22E−4, 4.58E−4, 7.69E−4, and 1.13E−3 counts s^{-1} $arcmin^{-2}$ for significance levels 3 σ, 4 σ, 6 σ, 8 σ, 12 σ, and 16 σ. N4406/N4374 (M86/M84): contour levels are 5.02E−4, 7.09E−4, 1.15E−3, 1.66E−3, 2.22E−3, 3.50E−3, 4.20E−3, 5.01E−3, 5.88E−3, 7.59E−3, and 8.66E−3 counts s^{-1} $arcmin^{-2}$ for significance levels 3 σ, 4 σ, 6 σ, 8 σ, 10 σ, 14 σ, 16 σ, 18 σ, 20 σ, 24 σ, and 26 σ. N4459: contour levels are 4.18E−4, 5.85E−4, 7.61E−4, 1.17E−3, 1.62E−3, and 2.10E−3 counts s^{-1} $arcmin^{-2}$ for significance levels 3 σ, 4 σ, 5 σ, 7 σ, 9 σ, and 11 σ. N4472: contour levels are 2.63E−4, 4.92E−4, 7.40E−4, 1.02E−3, 1.36E−3, 2.20E−3, 3.26E−3, 4.65E−3, 6.24E−3, 8.04E−3, 1.22E−2, and 1.45E−2 counts s^{-1} $arcmin^{-2}$ for significance levels 3 σ, 5 σ, 7 σ, 9 σ, 11 σ, 15 σ, 20 σ, 25 σ, 30 σ, 35 σ, 45 σ, and 50 σ. N4473/N4477: contour levels are 4.18E−4, 5.78E−4, 9.38E−4, 1.35E−3, 1.80E−3, and 2.28E−3 counts s^{-1} $arcmin^{-2}$ for significance levels 3 σ, 4 σ, 6 σ, 8 σ, 10 σ, and 12 σ.

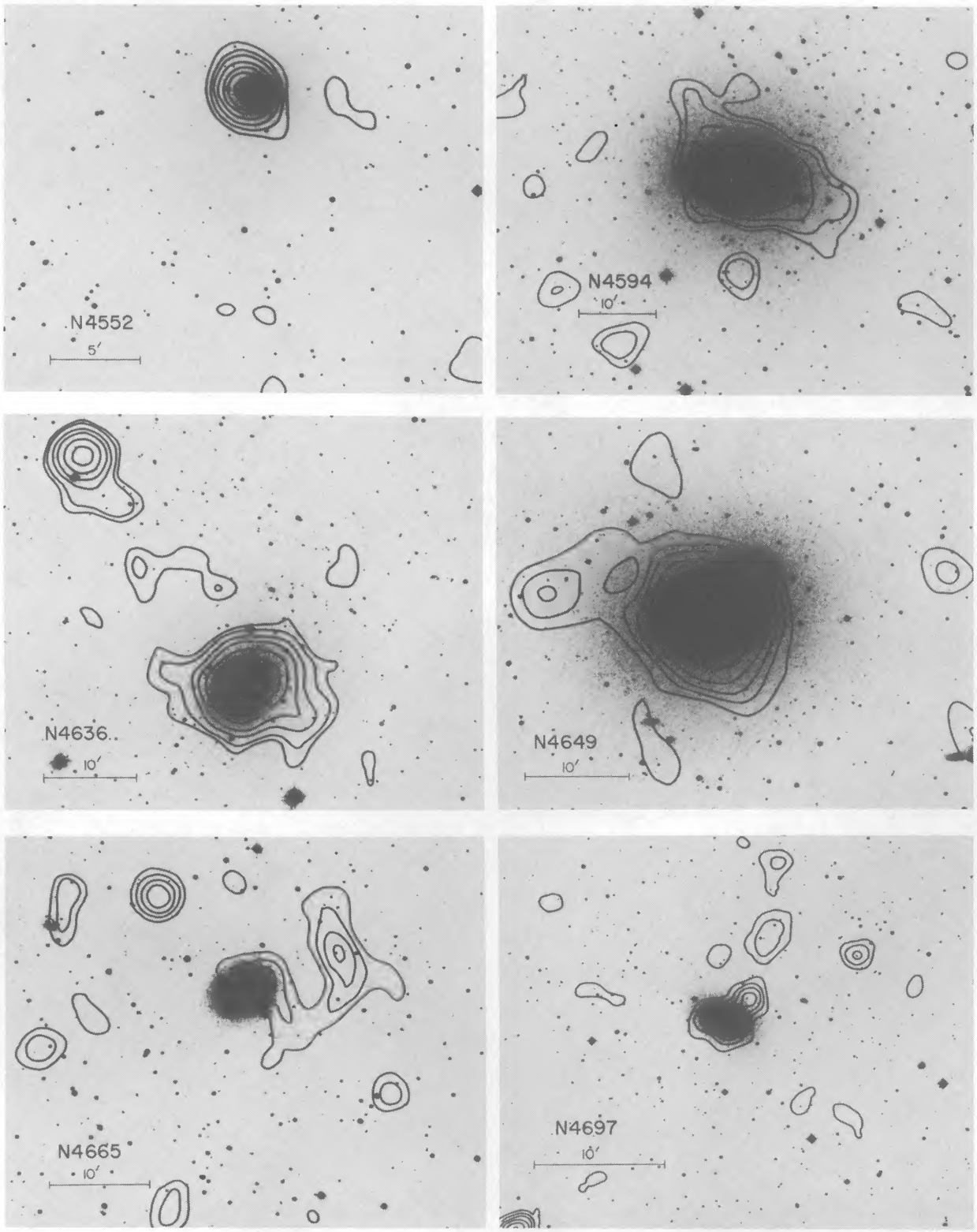

FIG. 1*d*.—N4552: contour levels are 3.11E−4, 5.54E−4, 8.42E−4, 1.32E−3, 1.87E−3, 2.45E−3, and 3.09E−3 counts s^{-1} $arcmin^{-2}$ for significance levels 3 σ, 5 σ, 7 σ, 10 σ, 13 σ, 16 σ, and 18 σ. N4594: contour levels are 2.82E−4, 3.98E−4, 6.69E−4, 1.00E−3, 1.83E−3, 2.85E−3, and 4.67E−3 counts s^{-1} $arcmin^{-2}$ for significance levels 3 σ, 4 σ, 6 σ, 8 σ, 12 σ, 16 σ, and 20 σ. N4636: contour levels are 8.39E−4, 1.22E−3, 2.10E−3, 3.18E−3, 5.15E−3, 7.55E−3, 1.03E−2, 1.35E−2, and 1.70E−2 counts s^{-1} $arcmin^{-2}$ for significance levels 3 σ, 4 σ, 6 σ, 8 σ, 11 σ, 14 σ, 17 σ, 20 σ, and 23 σ. N4649: (IPC) contour levels are 3.19E−4, 5.83E−4, 8.92E−4, 1.47E−3, 2.93E−3, 5.49E−3, 9.05E−3, and 1.38E−2 counts s^{-1} $arcmin^{-2}$ for significance levels 3 σ, 5 σ, 7 σ, 10 σ, 16 σ, 24 σ, 33 σ, and 43σ. N4665: contour levels are 2.32E−4, 3.19E−4, 4.12E−4, and 5.09E−4 counts s^{-1} $arcmin^{-2}$ for significance levels 3 σ, 4 σ, 5 σ, and 6 σ. N4697: contour levels are 3.12E−4, 4.42E−4, 5.84E−4, 7.38E−4, 9.03E−4, 1.07E−3, and 1.26E−3 counts s^{-1} $arcmin^{-2}$ for significance levels 3 σ, 4 σ, 5 σ, 6 σ, 7 σ, 8 σ, and 9 σ.

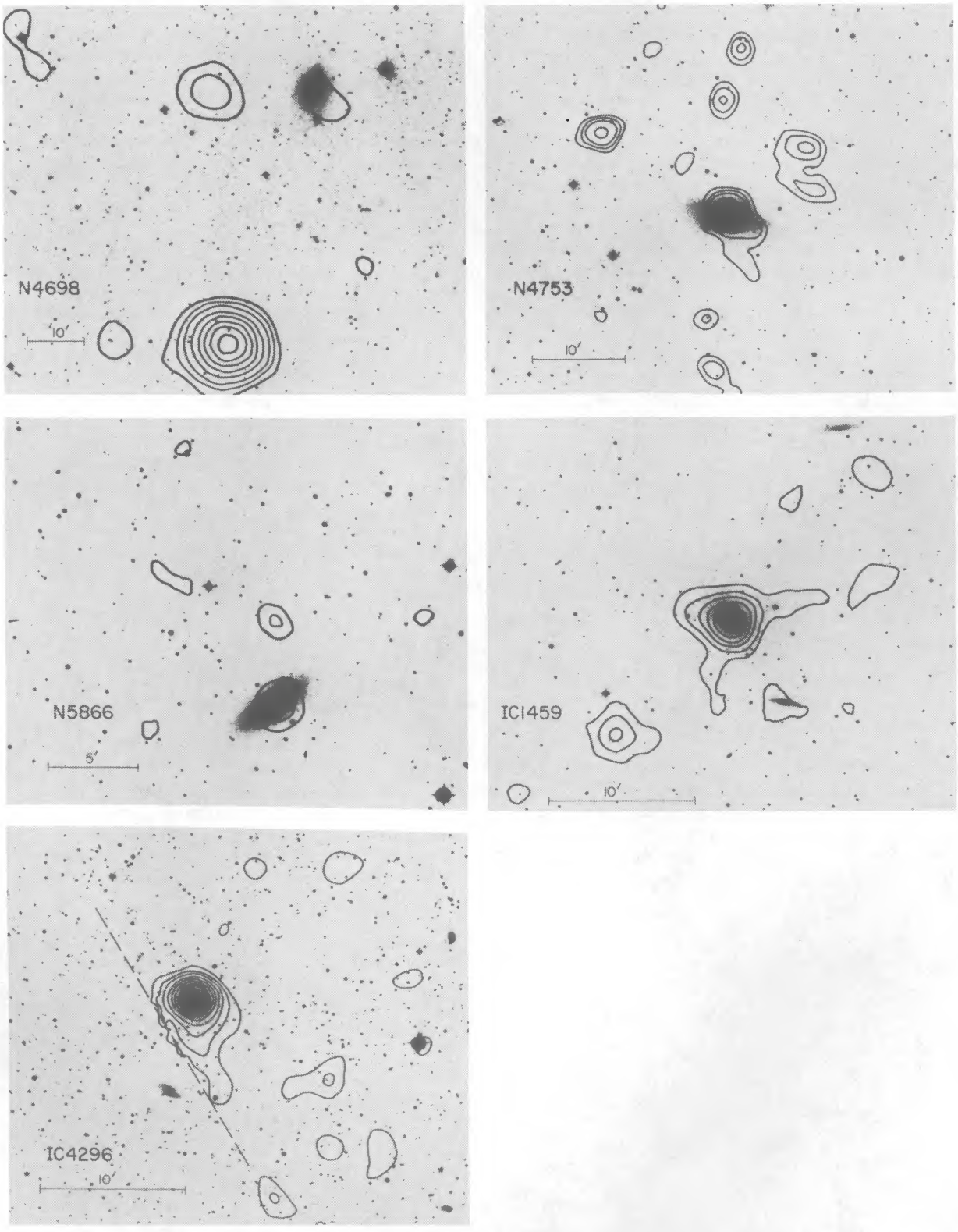

FIG. 1*e*.—N4698: contour levels are 3.60E−4, 6.63E−4, 1.20E−3, 1.70E−3, 2.47E−3, 3.34E−3, 4.29E−3 and 5.32E−3 counts s^{-1} $arcmin^{-2}$ for significance levels 3 σ, 5 σ, 7 σ, 10 σ, 13 σ, 16 σ, 19 σ, and 22 σ. N4753: contour levels are 2.71E−4, 3.56E−4, 4.42E−4, 6.28E−4, and 8.26E−4 counts s^{-1} $arcmin^{-2}$ for significance levels 4 σ, 5 σ, 6 σ, 8 σ, and 10 σ. N5866: contour levels are 4.98E−4, 7.20E−4, and 9.58E−4 counts s^{-1} $arcmin^{-2}$ for significance levels 3 σ, 4 σ, and 5 σ. IC 1459: contour levels are 1.80E−4, 3.42E−4, 5.40E−4, 7.75E−4, 1.04E−3, 1.33E−3, and 1.65E−3 counts s^{-1} $arcmin^{-2}$ for significance levels 3 σ, 5 σ, 7 σ, 9 σ, 11 σ, 13 σ, and 15 σ. IC 4296: contour levels are 2.42E−4, 4.33E−4, 6.62E−4, 9.06E−4, 1.18E−3, 1.46E−3, 1.78E−3, 2.09E−3, and 2.44E−3 counts s^{-1} $arcmin^{-2}$ for significance levels 3 σ, 5 σ, 7 σ, 9 σ, 11 σ, 13 σ, 15 σ, 17 σ, and 19 σ.

superposed on PSS or ESO prints of the optical galaxy (see Fig. 1). For the HRI images, we smoothed the data with a Gaussian of $\sigma = 20''$, while for the IPC observations we used $\sigma = 45''$. The majority of fields also were smoothed with smaller Gaussians to search for structure or point sources which might have been overlooked with the larger scale smoothings. For the smoothed data, a standard 1 σ uncertainty is approximately associated with each flux level. By measuring the background level in the image and computing the error associated with each level, we then plotted isointensity contours at various levels of significance. These are described in the captions for each galaxy in Figure 1 along with the corresponding flux levels in counts s^{-1} $arcmin^{-2}$. The lowest contour level shown is always three levels (3 σ) above the background.

We produced radial surface brightness profiles of each of the 13 galaxies (see Table 2) for which at least 100 photons were detected above the background. For the IPC observations we generated two sets of radial profiles with annuli of either 8′ or 24′ width. For the HRI observations we used annuli of 5′, 10′, and 20′. In generating the profiles, we assumed azimuthal symmetry and omitted regions containing serendipitous X-ray sources. We fitted the surface brightness distributions to models of the form

$$S(r) = S(0)[1 + (r/a)^2]^{-3\beta+1/2}, \quad (1)$$

where various values of the core radius a and the exponent $(3\beta - \frac{1}{2})$ were assumed. This form of the surface brightness distribution was chosen only to allow a convenient description of the density distribution. For the IPC observations each model was convolved with the instrument response. Each IPC model (nine values of $3\beta - \frac{1}{2}$ ranging from 0.7 to 2.5, and 22 values of a ranging from 20′ to 500′) was fitted to the radial surface brightness profile, and a χ^2 was determined. The minimum χ^2 in the array of models was found, and the allowed ranges for the core radius and exponent within 90% uncertainties were measured (Avni 1976). This procedure was carried out on both the 8′ and 24′ binnings of the IPC observations. Figure 2 shows four surface brightness profiles for galaxies in our sample. A similar procedure was performed on the HRI, except, because of the high spatial resolution of the instrument, the instrumental response was not convolved with the models. In Figure 3 we show profiles of three early-type galaxies compared with a point source (3C 273) as well as a late-type spiral galaxy (NGC 4579) whose X-ray emission is dominated by a nuclear source. All the HRI profiles of early-type galaxies are inconsistent with a single point source, as the figure suggests.

For Cen A, the analysis we performed differed from that described above. The *Einstein* imaging observations of Cen A have been discussed by Schreier *et al.* (1979) and Feigelson *et al.* (1981), who reported the detection of a hot corona. To obtain the surface brightness profile of the corona, we generated a background-subtracted radial profile for Cen A (omitting a 45° segment around the jet) and for a point source 4U 1658−48. Using the source counts within a 3′ radius, we normalized the point-source profile to Cen A's and determined the radial profile of the corona as the difference in the counts beyond 3′ (see Fig. 4). The slope of the profile agrees with that found for the other coronae in this sample. The observed X-ray luminosity of the corona outside 3′ is $\sim 5 \times 10^{39}$ ergs s^{-1}. If the profile of the emission inside 3′ is similar to the other coronae discussed here, the total X-ray luminosity of the corona would be 1.3×10^{40} ergs s^{-1}.

For the X-ray–bright galaxies (Table 2) we have quoted values for the best fit core radius to the surface brightness distribution. However, radiative cooling of the gas in the galaxy core may lead to a smaller observed core radius than the true value. If the gas is isothermal, then the surface brightness distribution of equation (1) can be directly inverted to yield the gas density distribution as

$$\rho_{gas}(r) = \rho_{gas}(0)[1 + (r/a)^2]^{-3\beta/2}. \quad (2)$$

In this case, the core radii determined by fitting the surface brightness distribution can be used to compute the central gas density. The resulting central densities for the 13 galaxies included in this analysis are typically above 10^{-2} cm^{-3}, with cooling times as short as 10^8 years. It is possible that energy input mechanisms and conduction serve to maintain a nearly isothermal distribution, although on scales of a few kiloparsecs

TABLE 2

DERIVED QUANTITIES FOR 13 X-RAY–BRIGHT GALAXIES

Galaxy[a] (NGC)	a (kpc)	β	R_{max} (kpc)	M_{gas}[b] ($M_\odot$)	$M_{gas}/M_{stellar}$[c]	M_{tot}[d] ($M_\odot$)	M_{tot}/L_B	R_{iso} (kpc)
315	≤5.4	≤0.7	110	6.47×10^{10}	0.050	5.7×10^{12}	26	86
1316	1.4 ± 0.5	0.5 ± 0.1	34	3.27×10^{9}	0.002	2.0×10^{12}	8	29
1332	≤2.8	0.6 ± 0.1	36	2.47×10^{9}	0.010	2.5×10^{12}	62	20
1395	≤6.5	≤0.45	98	1.96×10^{10}	0.056	5.1×10^{12}	88	49
2563	≤8.8	≤1.0	80	3.02×10^{10}	0.074	4.1×10^{12}	60	80
4374	2.0 ± 0.5	0.5 ± 0.1	15	7.84×10^{8}	0.002	8.6×10^{11}	14	...
4382	≤4.0	≤0.45	48	3.05×10^{9}	0.007	2.5×10^{12}	37	22
4406	3 ± 1	0.45 ± 0.05	88	2.54×10^{10}	0.058	4.6×10^{12}	63	86
4472	1.5 ± 0.5	0.5 ± 0.05	80	2.09×10^{10}	0.025	4.6×10^{12}	33	62
4594	≤9.3	≤0.65	32	3.25×10^{9}	0.003	1.7×10^{12}	8	25
4636	1.6 ± 0.5	0.45 ± 0.05	44	7.73×10^{9}	0.049	2.3×10^{12}	87	44
4649	≤2.0	0.5 ± 0.05	36	5.06×10^{9}	0.010	2.1×10^{12}	24	30
5128	...	0.5 ± 0.1	20	6.64×10^{8}	0.001	1.2×10^{12}	7	16

[a] All the galaxies were observed with the *Einstein* IPC, and NGC 315, 1316, 4374, 4406, 4472, 4636, 4649, and 5128 were also observed with the HRI.

[b] When an upper limit on the core radius is given, this was used to estimate the mass in gas. As noted in the text, the total gas mass is relatively insensitive to the core radius. If an upper limit on β is given, we used $\beta = 0.45$.

[c] For computing the ratio of M_{gas} to $M_{stellar}$, we used $M_{stellar}/L_B = 6$ to convert from L_B to $M_{stellar}$. We used 5.48 as the absolute magnitude for the Sun (Tammann 1982).

[d] For computing the total mass, we have assumed an isothermal gas temperature of 1.2×10^7 K. If an upper limit on β is given, we used $\beta = 0.45$.

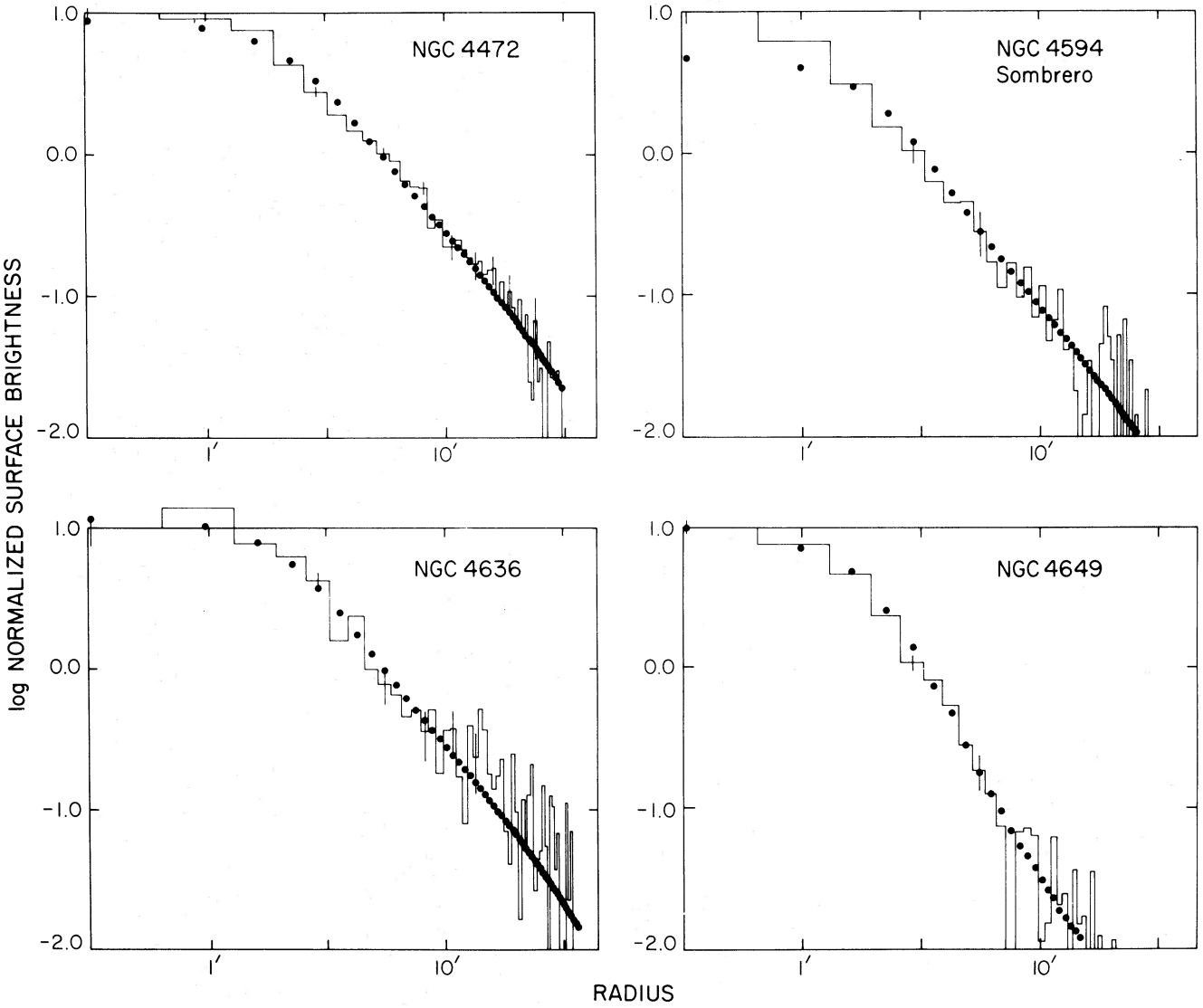

FIG. 2.—The radial surface brighteness profiles for four galaxies in this sample obtained with the *Einstein* IPC are shown, as well as the best fit model

radiative cooling may produce a temperature gradient (Nulsen, Stewart, and Fabian 1984). Since the X-ray emissivity of the gas increases with decreasing temperature (over the temperature range from 10^5 to 4×10^7 K; e.g., see McKee and Cowie 1977), a positive temperature gradient ($dT/dr > 0$) in the galaxy core would serve to decrease the apparent core radius artificially, yielding spuriously small core radii and high central densities. Thus, the core radii, if used to describe the density distribution (eq. [2]), should be considered as lower limits.

For observations of an additional 15 galaxies from which fewer than 100 photons but more than 30 were obtained, we compared the ratios of source counts in different annuli to that in a point source. Table 3 shows that the X-ray emission from all but two of these galaxies (NGC 1533 and NGC 4552) is inconsistent with a point source. The extended nature of the emission from these galaxies is also apparent in many of the isointensity contours shown in Figure 1.

As the fourth stage in our analysis, we used the pulse-height data of the IPC to determine the allowed parameters of both thermal (Raymond, Cox, and Smith 1976) and power-law spectra. We are interested only in measuring the temperature of the gas and have therefore used the hydrogen column densities (Table 4, col. [2]) determined from Heiles (1975) or Daltabuit and Meyer (1972). We have allowed the hydrogen column density to be up to a factor of 2 higher than the nominal value to take into account the possibility of absorption from material in dense clouds along the line of sight which contribute to the X-ray but not to the radio (H I) column density. The values of the temperature are given in column (3) of Table 4, and the range corresponds to a 90% confidence interval for one interesting parameter, the temperature ($\Delta\chi^2 = 2.7$; Avni 1976). The value of the minimum χ^2 and the number of degrees of freedom also are given in Table 4. For all our observations we used the uniform IPC illumination to correct for gain variations over the field (as appropriate to extended sources). For NGC 4374 and NGC 4406 we give two temperature determinations in Table 4, based on two separate observations for the galaxies and for the plume above NGC 4406. The field centers of the two observations differ by almost 15′, and the detector gains by nearly half the operating range.

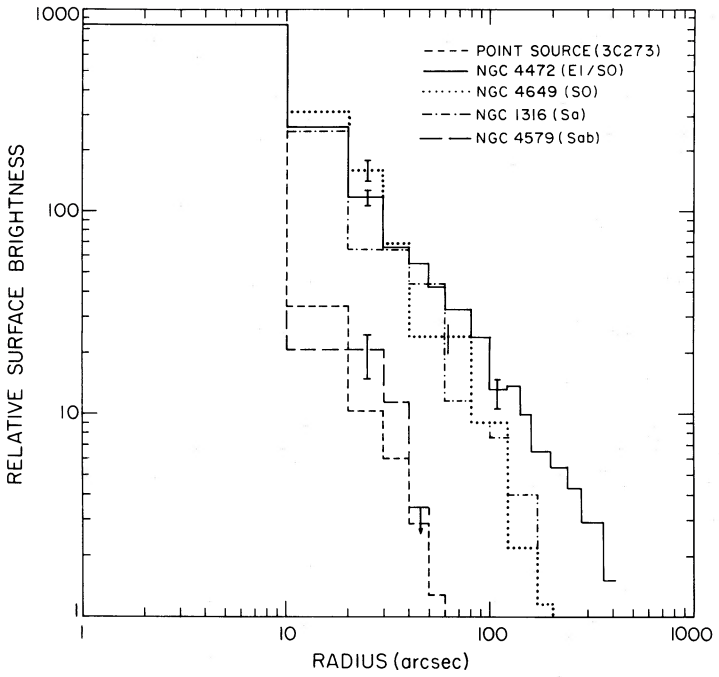

FIG. 3.—The radial surface brightness profiles obtained with the *Einstein* HRI are shown for three early-type galaxies, as well as for the quasar 3C 273 and the spiral galaxy NGC 4579, in which the dominant emission is due to a point source at the nucleus. The profiles have been normalized to each other, based on the flux in the central bin. The extended nature of the emission from the early-type galaxies is apparent.

The resulting pairs of best-fit values of the temperature for NGC 4374 and NGC 4406 agree to within 0.25 keV and are consistent within the reported errors.

In addition to thermal fits, we also performed power-law fits to the IPC pulse-height data. The sources with fewer total counts gave acceptable values of χ^2. However, in contrast to the thermal fits, all of which were acceptable, several of the $\chi^2_{\rm min}$ values of the power-law spectra for the stronger sources are unacceptably high. For a power-law description of the energy spectrum, NGC 4406 gives minimum χ^2 values of 260 and 51 for 8 and 7 degrees of freedom (for the two separate observations), respectively; NGC 4472 gives $\chi^2 = 60$ for 7 degrees of freedom; NGC 4636 gives $\chi^2 = 16.8$ for 8 degrees of freedom; and NGC 4649 gives $\chi^2 = 14.4$ for 7 degrees of freedom. Thus, individually several of the galaxies are poorly described by power-law spectra, and as a group they are better characterized by a thermal emission mechanism.

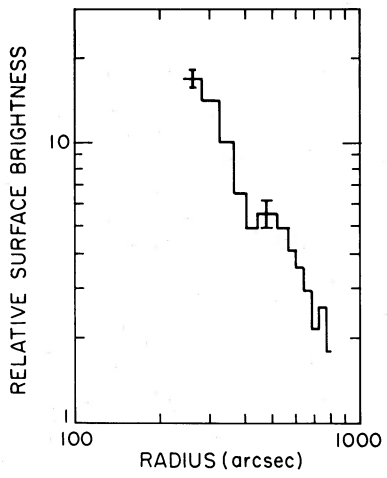

FIG. 4.—The radial surface brightness profile of the corona around Cen A is shown. This was obtained by normalizing the source counts within a 3′ radius central region to those of a point source. The radial profile of the point source beyond 3′ was then subtracted from the surface brightness profile for Cen A, and the remainder is plotted in this frame.

The results of our spectral analysis (Table 4) show that the coronae range in temperature (assuming a thermal mechanism) from ~ 0.5 to ~ 2 keV, although some values are given only as lower limits (e.g., NGC 4382). The best measured temperatures (NGC 4374, NGC 4406, NGC 4472, NGC 4636, NGC 1395) lie in this range and are consistent with a single temperature of ~ 1 keV (allowing for systematic uncertainties and possible variations of the hydrogen column density as noted above).

Given that the coronae are produced by radiation from an isothermal diffuse hot gas (see below for detailed justification) and are, in general, spherically symmetric, we can compute both the gas density and the integrated gas mass as a function of radius. For our galaxy sample, total observed gas masses range from $\sim 5 \times 10^8$ to $\sim 5 \times 10^{10}\ M_\odot$. The uncertainty in the gas mass resulting from the uncertainty in the true core radius is, fortunately, small. Decreasing (increasing) the core radius by a factor of 10 changes the total gas mass by roughly 10% (25%). For coronae with measured surface brightness profiles (i.e., core radii and β), Table 2 gives the maximum radius to which X-rays have been detected ($R_{\rm max}$) and the total observed gas mass, $M_{\rm gas}$, required to produce the observed luminosity. Using a mass-to-light ratio of 6 (which is appropriate for the stellar material; see Faber and Gallagher 1979), we have converted the absolute blue magnitudes given in Table 1 to mass. The mass of the optically luminous matter, $M_{\rm stellar}$, verted the absolute blue magnitudes given in Table 1 to mass. The mass of the optically luminous matter, $M_{\rm stellar}$, has been

TABLE 3

COMPARISON OF THE RADIAL DISTRIBUTIONS OF 15 SAMPLE GALAXIES WITH A POINT SOURCE

Galaxy	Ratio of Counts in Annuli of 0′–80′ and 80′–160′	Galaxy	Ratio of Counts in Annuli of 0′–80′ and 80′–160′
Point source	5.07	NGC 4459	1.24 ± 0.51
NGC 524	1.21 ± 0.38	NGC 4473	0.55 ± 0.16
NGC 1533	5.18 ± 1.92	NGC 4477	0.73 ± 0.20
NGC 1600	2.43 ± 0.99	NGC 4552	5.24 ± 2.02
NGC 2300	2.39 ± 0.86	NGC 4665	1.19 ± 0.31
NGC 3258	0.57 ± 0.17	NGC 4753	1.57 ± 0.35
NGC 3585[a]	1.21 ± 0.35	IC 1459	2.35 ± 0.71
NGC 4365	2.19 ± 0.48	IC 4296	2.46 ± 0.64

[a] Extended nature may be due to emission of nearby elliptical galaxy (see Fig. 1).

has been used to compute the ratio of gas mass to stellar mass in Table 2. The fraction of mass in the X-ray corona ranges up to 7% of the mass in stars and therefore contributes little to the total galaxy mass. (If we had used a mass-to-light ratio of 10, the largest measured fraction of gas mass to stellar mass would have been 4%.) Table 2 also gives isophotal radii measured at 2.5×10^{-4} IPC counts s^{-1} arcmin^{-2}.

III. DISCUSSION: X-RAY CORONAE AS A PROBE OF THE MASS DISTRIBUTION IN EARLY-TYPE GALAXIES

X-ray coronae are a common feature of early-type galaxies. Figure 5 shows the relationship between absolute blue magnitude and X-ray luminosity for the galaxies listed in Table 1. In general, Figure 5 shows a clear correlation such that optically more luminous galaxies are more luminous in X-rays (see also Long and Van Speybroeck 1983 and Trinchieri and Fabbiano 1984 for a comparison of early- and late-type galaxies). The coronae may be powered by each galaxy's supernovae, which in the absence of a cool interstellar medium convert their kinetic energy into heat in the corona. Thus, more luminous galaxies can power and bind more luminous coronae. Several galaxies which tend to fall below the general correlation of M_B-L_x also can be understood in this context. Cen A, for example, in spite of its high optical luminosity, cannot support an extensive corona because much of its supernova energy is dissipated in its optically observed cool interstellar medium and thus the supernova energy is unavailable for conversion to heat in its corona (see McKee and Ostriker 1977). In addition, there is a tendency for the Sa galaxies (as a class, those with some cool interstellar medium) to have lower X-ray luminosities compared with their optical luminosities and, thus, less extensive coronae (Table 2, Fig. 5) than do elliptical galaxies. In a subsequent paper we discuss these energy-balance questions in detail and show that galaxies with extensive cool inter-

TABLE 4

SPECTRAL FITS

Galaxy	Hydrogen Column Density ($\times 10^{20}$ cm^{-2})[a]	Temperature (keV)[b]	χ^2_{min}	Degrees of Freedom[c]
NGC 1395	< 1.60	0.51–0.90	11.3	8
NGC 4374[d]	3.35	0.79–2.53	6.8	8
		0.93–1.32	3.8	7
NGC 4382	2.37	> 0.80	14.7	7
NGC 4406[d,e]	3.35	1.13–1.93	5.2	8
		0.94–1.03	3.8	7
NGC 4427 (total):	1.64	1.07–1.30	3.6	7
Ring 0′–180′		1.01–1.25	1.7	7
Ring 180′–300′		0.95–1.38	4.1	8
Ring 300′–650′		1.25–3.5	12.4	8
NGC 4594	3.83	> 1.6	5.2	7
NGC 4636	< 1.89	0.78–1.21	6.7	8
NGC 4649	2.41	1.78–4.12	5.2	7

[a] Nominal hydrogen column density. We allowed the actual column density to range up to twice the nominal value to account for the possibility of dense clouds along the line of sight. 90% confidence range.

[b] 90% confidence range.

[c] Data points less two parameters (normalization and temperature).

[d] Two separate observations of NGC 4374 and NGC 4406 are available (sequence numbers 4311 and 278). They are at different instrumental gains, and the positions of the galaxies in the detector differ. Therefore, these observations serve to verify our analysis in correcting for gain variations from field to field and within each field.

[e] The fits given refer to both the emission centered on the galaxy and that in the plume to the north (see Fig. 1). The plume and the galaxy itself, separately, give comparable thermal fits. The plume has a temperature (90% confidence range) of 0.95–1.43 and 0.77–0.93 keV for each of the two separate observations. The corresponding values for the galaxy alone are 0.85–1.23 and 0.67–0.80 keV.

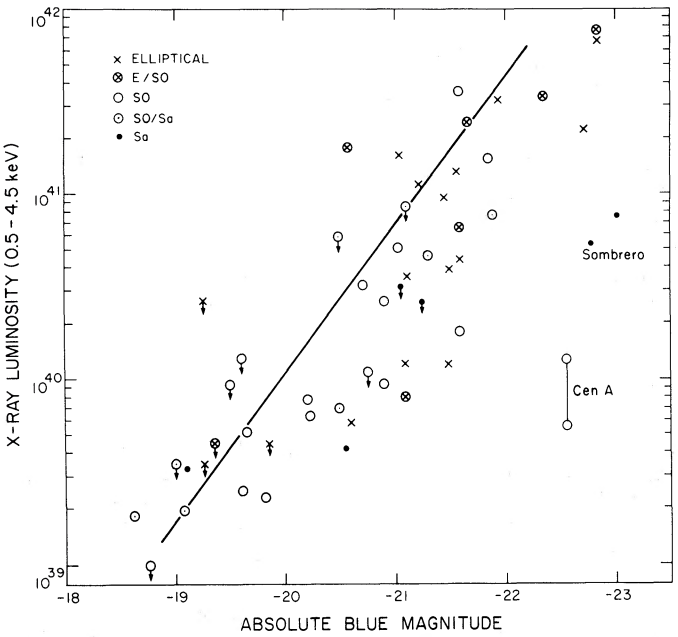

FIG. 5.—The 0.5–4.5 keV X-ray luminosity is plotted against the galaxy blue magnitude for the sample in Table 1. Symbols denote different galaxy morphologies (Sa, S0, E). The line is not a fit to the data but is the L_x-L_B correlation (and normalization) predicted if all the X-ray emission arises from thermal bremsstrahlung of hot gas produced by stellar evolution at the rate of 0.015 $M_\odot$ yr^{-1} per 10^9 $L_\odot$ for 10^{10} years and stored in a halo with a surface brightness profile comparable to those observed. Note that if the distance to Cen A were less, its plotted location would lie closer to the general distribution.

stellar media do not have hot galactic coronae because the supernova energy can be dissipated in the cool material.

One of the most important questions which the X-ray observations allow us to address is the mass of elliptical (and S0) galaxies. Because early-type galaxies lack the tracers which have been used to determine dynamical masses of later type (spiral) galaxies to large galactocentric distances, the total masses of early-type galaxies are poorly known (see Faber and Gallagher 1979 for a review). For elliptical galaxies, relatively few long-slit spectra have been obtained to determine the velocity dispersion as a function of radius (e.g., Davies and Illingworth 1983), and except for the exceptional cD systems (Dressler 1979; Carter *et al.* 1984) the rapid decrease in the optical light prevents the determination of dynamical masses on scales comparable to those studied in spiral galaxies. Thus, many mass-to-light determinations for elliptical galaxies rely on extrapolations of centrally measured velocity dispersions. X-ray observations which detect gas at radii up to $\sim$100 kpc from the centers of galaxies (well outside the Holmberg radius) can provide the needed probe to study the mass distributions of early-type galaxies at large radii.

a) Assumptions and Justifications

The use of the X-ray observations as a probe of the mass distribution at large radii rests on several premises, which we argue below are well founded. We discuss first the thermal bremsstrahlung nature of the emission, second the quasi-hydrostatic nature of the coronae, and third the unimportance of pressure confinement.

i) Thermal Emission

Several arguments provide strong evidence that the emission from the X-ray coronae is produced predominantly by radiation from a hot gas surrounding the galaxy. First, the X-ray spectra themselves are all consistent with the thermal emission from hot gas at $\sim$1 keV as characterized by the Raymond, Cox, and Smith (1976) code, and those with sufficient statistics are inconsistent with nonthermal, power-law spectra. Observations at other wavelengths as well as the extended nature of the X-ray emission also argue against nonthermal mechanisms for the emission. In particular, the galaxies are normal in the sense that they generally have typical absorption-line spectra with no unusual emission features which would indicate high ionization levels. Of the galaxies in our sample whose X-ray emission is unresolved, only NGC 3593 is known to have pronounced emission lines from Hα and [N II] (Huchra 1984). In addition, many of the galaxies with coronae are not detected as radio sources. For four galaxies containing radio sources, *Einstein* HRI observations place limits on the contribution to the total emission from a nuclear point X-ray source of less than 4% for NGC 1316 and NGC 4472, less than 10% for NGC 315, and less than 16% for NGC 4374. Thus, the evidence for a substantial contribution to the X-ray emission from nuclear activity is minimal for those sources which we do not resolve. We note, however, that a large fraction of early-type galaxies do show weak optical emission lines (Caldwell 1982). This cool material may represent that in a small cooling flow which might be expected in the centers of the coronae (Nulsen, Stewart, and Fabian 1984).

While the nonspherical structure of several of the X-ray sources and the lack of agreement between the spatial distribution of the X-ray and optical emission (e.g., NGC 4406 [M86] and NGC 1332) argue against emission from the integrated populations of galactic type X-ray sources (see Fig. 1), the predicted integrated luminosities are also too low to account for the observed levels. Since elliptical galaxies are often associated with large numbers of globular clusters located in a galactic halo, we examined the contribution these might make to the observed emission. Using the total luminosity of globular clusters in our galaxy (Hertz and Grindlay 1983), we find a mean X-ray luminosity of 1.3×10^{36} ergs s^{-1} per cluster. The mean X-ray luminosity of globulars in M31 is higher, about 4×10^{36} ergs s^{-1} (Van Speybroeck 1984). Taking the number of globular clusters as 2500 per bright galaxy (e.g., M86, M84; see Harris and Racine 1979), we predict a total X-ray luminosity of about 10^{40} ergs s^{-1} from globular cluster emission, which is less than the observed luminosity for these galaxies. Furthermore, the X-ray energy spectra of globular clusters are harder ($kT \sim 5$ keV; Hertz and Grindlay 1983) than those observed for the coronae.

Feigelson *et al.* (1981) discussed the discrete-source hypothesis for the diffuse emission observed from Centaurus A. For main-sequence stars, the preponderance of M dwarfs in elliptical galaxies (Spinrad and Taylor 1971) makes them the primary contributors to the X-ray luminosity. Feigelson *et al.* note that to account for the diffuse X-ray emission, these stars in Cen A must all have luminosities at the peak of the range found in our own galaxy for Population I M dwarfs. However, the evidence suggests that their Population II counterparts, the relevant population in Cen A, are much less luminous (up to 10–100 times fainter; Rosner 1984). For luminous X-ray sources, Feigelson *et al.* (1981) argued that the Population II type (galactic bulge) sources show a preference for high stellar

density regions. Such a trend would require the X-ray emission to be more concentrated than the optical light, and yet the opposite is observed. For example, at large radii the optical surface brightness envelopes of elliptical galaxies fall *faster* than r^{-2} (e.g., Thuan and Romanishin 1981), while the X-ray profiles are well described at large radii by $r^{-1.7}$. In addition, as with the globular cluster sources, galactic bulge sources have harder spectra (Jones 1977) than we observe for the coronae.

Feigelson *et al.* (1981) conclude that the most promising origin for the diffuse emission from Centaurus A is radiation from a diffuse hot gas. We agree with this interpretation, for the reasons detailed and reviewed above. However, even if we assume that some portion of the diffuse emission from Cen A arises from stellar/compact sources, then, because of the high optical luminosity of Cen A and its relatively low X-ray emission, this provides a stringent limit on the integrated contribution of discrete sources in early-type galaxies. An assumed contribution from discrete sources of 50% of the diffuse Cen A X-ray emission (1.3×10^{40} ergs s^{-1}) combined with an absolute magnitude of $M_B = -22.6$ yields an upper limit to the discrete-source X-ray emission from early-type galaxies (Population II stellar systems) of 4×10^{37} ergs s^{-1} per $10^9\ L_\odot$. Assuming that this value does not vary with optical luminosity, one finds that only the faintest galaxies ($M_B \gtrsim -19$) in our sample could have a substantial contribution from discrete-source emission, while for the most optically luminous galaxies the discrete-source contribution is at most $\sim 2\%$ of the galaxy emission. Thus, the bulk of the emission from all but the faintest early-type galaxies in our sample does not originate from the integrated X-ray emission of known types of individual stellar/compact sources.

Another argument in favor of a diffuse-gas origin for the emission results from the dependence of the X-ray emission on the optical luminosity (see Fig. 5). Most models of emission from discrete sources predict that the number of X-ray–emitting objects would be proportional to the optical luminosity (or galaxy mass, since $M/L \sim$ constant). The color of elliptical galaxies shows no strong correlation with absolute magnitude (Sandage and Visvanathan 1978), and, hence, there is no evidence for population changes. Thus, if the dominant contribution to the X-ray luminosity of early-type galaxies were from discrete sources comprising a constant fraction of the galaxy mass, then the X-ray luminosity should be linearly proportional to the optical luminosity, as is observed for spiral galaxies (Fabbiano, Trinchieri, and Macdonald 1984). However, the actual dependence of L_x on L_B is steeper than linear. The line drawn in Figure 5 is $L_x \propto L_B^2$.

The origin of the steep dependence of L_x on L_B can be derived from a variety of possible scenarios if the emission is produced by a hot gas. Most simply, if we assume that all the galaxies have the same (or nearly the same) underlying mass distributions (with a potential corresponding to the observed surface brightness distribution with $r_c = 2$ kpc and $\beta = 0.45$ out to a maximum radius of 50 kpc), and that mass is lost by stars at the rate of 0.015 $M_\odot$ yr^{-1} per $10^9\ L_\odot$ (Faber and Gallagher 1976) and is accumulated for $\tau_{10} \times 10^{10}$ years, then

$$L_x = 5.2 \times 10^{37} (\tau_{10} L_9)^2 \text{ ergs s}^{-1} . \quad (3)$$

This is the line drawn in Figure 5.

Alternatively, other scenarios include the following:

1. The supernova luminosity (i.e., supernova rate) depends on galaxy mass (galaxy luminosity) according to $L_{SN} \propto L_B^2$.
2. The temperature dependence of the coronae on L_B is such that at low optical luminosity we have sufficiently low temperatures that the bulk of the emitted energy falls outside our energy band.
3. Other energy-loss processes are effective (e.g., galactic winds; in low optical luminosity galaxies much of the supernova energy is carried away in a wind).
4. As suggested by Nulsen, Stewart, and Fabian (1984), if the only energy source is that from gravitational accretion, then $L_x \propto L_B^{5/3}$, where we have used the luminosity-velocity dispersion relation, $L_B \propto \sigma^3$, as derived by Tonry (1982) and Dressler (1984).

These possibilities are explored in greater detail in a subsequent paper, where we investigate the energy and mass balance of the coronae.

ii) *Hydrostatic Equilibrium*

The basic arguments in favor of hydrostatic equilibrium can be derived from the observability of the gaseous coronae. First, if the gas were isothermal and freely expanding, we would expect a gas density profile proportional to r^{-2}, where r is the galactocentric distance, and a steeper profile if the gas is adiabatically cooling. Instead, flatter profiles ($r^{-1.5}$) are observed. Also, the mass of gas required to replenish an expanding corona cannot be replaced on the necessary time scales by any reasonable processes. In an outflow, or galactic wind scenario, for the typical case explored by MB, the total mass within a galactic radius is $7.7 \times 10^7\ M_\odot$, and the time to sweep a given fluid element from the center to the edge of the galaxy is 4×10^7 years (corresponding to their assumed stellar mass loss rate of a few solar masses per year). However, the observed coronae have luminosities up to 10^6 times larger than that of the MB wind and gas masses up to 10^3 times larger (Table 2). Hence, mass loss rates, to produce a steady state flow, must be as high as several hundred solar masses per year, which is 2 orders of magnitude higher than typical estimates. A non–steady state scenario (e.g., Sanders 1981) where gas could be accumulated and then heated and expelled also can be ruled out, since the coronae are found in a large fraction, if not all, of the bright elliptical galaxies.

Infall models require that heat sources be unable to replenish the energy radiated. Supernovae can provide a significant energy source for powering the coronae, as we discuss in a subsequent paper. Even if we are to ignore any heat sources, the coronae can be shown to be in hydrostatic equilibrium outside the galaxy core, i.e., $(V_{cool}/C_s)^2 \ll 1$, where V_{cool} is the infall velocity of the radiatively cooling gas and C_s is its sound speed. We find

$$(V_{cool}/C_s)^2 = 1.1 \times 10^{-5} R_{22}^2\, n_{-3}^2\, T_7^{-4.2} , \quad (4)$$

where T_7 is the gas temperature in units of 10^7 K at a radius of R_{22} in units of 10^{22} cm, n_{-3} is the gas density in units of 10^{-3} cm^{-3}, and V_{cool} is the radius divided by the gas cooling time, which we derive using the emissivity taken from McKee and Cowie (1977). We assumed that the gas density can be roughly determined from our surface brightness profile as

$$n_{-3} \approx 100 R_{22}^{-1.5} , \quad (5)$$

with the core radius conservatively taken as 3 kpc (the larger core radius giving a higher density at larger radius). Therefore, we find

$$(V_{cool}/C_s)^2 \approx 0.11 T_7^{-4.2} R_{22}^{-1} , \quad (6)$$

and thus, for regions outside the core, the gas is effectively in hydrostatic equilibrium.

White and Chevalier (1984) have developed accretion models for gaseous coronae with and without massive halos. The coronal gas at 100 kpc has temperatures of $\sim 10^7$ K and, in the absence of an external confining cluster medium and a dark halo, would flow away from the galaxy at the gas sound speed. These models may be appropriate for slow-moving galaxies in clusters where the galaxy corona is pressure-confined by an external cluster medium. Some of the galaxy coronae discussed by Bechtold *et al.* (1983) may be of this kind. The models with dark halos may apply to galaxies in less dense regions where no substantial intergalactic medium exists.

Bregman (1984) has shown that a galactic wind will be produced if the gas temperature of a corona exceeds a critical temperature, $T_{\rm crit}$, approximately given by

$$T_{\rm crit} = 1.2 \times 10^6 M_{11}/r_{500} \text{ K} , \quad (7)$$

for a galaxy of 100 kpc radius and a King profile, where M_{11} is the total galaxy mass in units of $10^{11}\ M_\odot$ and r_{500} is the core radius of the gravitating mass in units of 500 pc. Since the coronae have temperatures of ~ 1 keV (1.2×10^7 K), the galaxy masses necessary to bind the gas are at least of the order of $10^{12}\ M_\odot$. The temperature criterion is determined at the galaxy center. Thus, if the gas temperature is ~ 1 keV in the outer regions, the gas will require even larger gravitational mass to remain bound. Thus, equation (7) gives the minimum mass required to suppress a galactic wind, and any infall models require masses at least this large. If the optical luminosity is proportional to the mass of a galaxy, then there is some optical luminosity below which galaxies lack sufficient mass to bind a hot (10^7 K) corona. Suppose that the total mass-to-light ratio of early-type galaxies is ~ 100: then eq. (7) implies that galaxies (with $r_{500} = 1$) fainter than $M_B \approx -18$ cannot maintain a hot corona.

iii) *Unimportance of Pressure Confinement*

If we can determine both the density and temperature gradients of the gas in the galaxy halo, then, even in the presence of a confining medium, our analysis will yield the total gravitating mass. However, since the galaxies in our sample have only limited or no information for the temperature gradient, it is important to verify that pressure confinement by an external medium is not important.

The density and temperature of a hot intergalactic medium (IGM) can be bounded by attributing *all* of the observed X-ray background to thermal bremsstrahlung radiation from a hot IGM. Gould (1980) has revised the emissivity from hot gas, and Fabian and Khembavi (1982), after subtracting a noncosmologically evolving active galaxy component, has derived a gas temperature and density. Their present epoch values ($z = 0$) are $T_{\rm IGM} = 8$ keV and $n_{\rm IGM} = 1.3 \times 10^{-7}$ cm^{-3}. A typical galaxy corona has a temperature of 1 keV and a central density of 10^{-2} (with a core radius of 2 kpc). With these parameters, the cool (isothermal) corona and the hot IGM come to pressure equilibrium at a galaxy radius of 200 kpc. The actual radius is probably even larger, since emission from clusters of galaxies contributes to the hard X-ray background ($\sim 10\%$), and active galaxies (QSOs) are an evolving population and may produce a large fraction of the X-ray background, thus reducing the allowed IGM density. Therefore, the possible pressure confinement effects of a hot IGM are small on the scales we are currently observing. Any much cooler IGM would have to have an unreasonably high density (compared with closure density) if it were to exert a significant pressure. Furthermore, the sound speed in the confining medium must exceed the random velocity of the galaxies if the confinement is to be effective over the entire surface of the corona.

Another possible confining medium is the intracluster gas in rich clusters. Although a large fraction of the galaxies in our sample are members of the Virgo Cluster, many of them are so far from the cluster core that the effect of the gas surrounding M87 is negligible. For two galaxies, NGC 4406 (M86) and NGC 4374 (M84), the cluster gas does significantly affect the coronae (see Fig. 1). The high velocity of NGC 4406 with respect to the mean of the Virgo Cluster suggests that the intracluster medium cannot effectively pressure-confine the gas. Instead, it provides an important ram pressure force. As Fabian, Schwarz, and Forman (1980) have emphasized for NGC 4406, the maintenance of an extensive corona against the ram pressure of the external medium requires that the galaxy have a massive dark halo. For pressure confinement to be important, not only must the velocities of Virgo galaxies with respect to the cluster mean be small ($\sim 20\%$ of the cluster velocity dispersion), but thermal conduction would need to be suppressed to prevent the evaporation of the coronae. Thus, for the galaxies in our sample, cluster gas also does not play a major confining role.

b) Mass Determinations

The above discussions have shown that the galactic coronae in the poor groups and cluster outskirts are not extensively pressure-confined by a hot external medium. Ideally one would address the problem of determining the total gravitating mass as a function of galaxy radius by constraining the radial temperature and density gradients of the gas. Then, using the equations of hydrostatic equilibrium, one can derive the gravitating mass required to give the observed X-ray surface brightness profiles.

Assuming that the X-ray–emitting gas is in hydrostatic equilibrium and is spherically symmetric, and that the gas obeys the ideal-gas law, one finds (e.g., Fabricant and Gorenstein 1983)

$$M(r) = \frac{-kT_{\rm gas}}{G\mu m_{\rm H}} \left(\frac{d \log \rho_{\rm gas}}{d \log r} + \frac{d \log T_{\rm gas}}{d \log r} \right) r , \quad (8)$$

where $\rho_{\rm gas}$ and $T_{\rm gas}$ are density and temperature, G is the constant of gravitation, $m_{\rm H}$ is the mass of the hydrogen atom, μ is the mean molecular weight of the gas, r is the radial distance, and $M(r)$ is the *total* gravitating mass within a radius r, which will, in general, be much greater than the X-ray emitting gas.

To determine $M(r)$ unambiguously, we need to determine the gas temperature and gas density gradients in the corona. We investigated the range of possible temperature gradients by parameterizing the temperature profile by

$$T(r) = T_0[1 + (r/r_T)]^{-\alpha} , \quad (9)$$

where $T(r)$ is the temperature at radius r, T_0 is the central temperature, and r_T is some characteristic radius which is small compared with the density core radius r_c. With equations (2) and (9) and for r large compared with r_c and r_T, we can write equation (8) as

$$M(r) = 3.2 \times 10^{11}(3\beta + \alpha) T_7 r_{10}\ M_\odot , \quad (10)$$

where T_7 is the gas temperature in units of 10^7 K at a radius r_{10} measured in units of 10 kpc. Our principal goal is to use observations of the temperature and density gradients at some large radius to estimate a lower limit to the total mass required in the galaxy halo. This is accomplished by having a temperature increasing with radius ($\alpha < 0$).

Only NGC 4472 is sufficiently luminous and nearby to provide us with spatially resolved spectral data (see Table 4). In Figure 6 we have plotted the temperature determined from the observed X-ray spectrum against that from the maximum allowed temperature gradient. Our fitting procedure involved numerically integrating the predicted temperature and density profiles and comparing these with the observed surface brightness profiles and the gas temperature observed for each radial region and for the total emission.

The free parameters of our modeling are β, r_c, ρ_0 (for the gas density distribution) and α, T_0 (for the gas temperature distribution), all of which affect the surface brightness profile. The central gas density, ρ_0, was used to normalize the observed and calculated surface brightness profiles and was treated as an "uninteresting" parameter (Avni 1976). Therefore, acceptable surface brightness profiles were defined as those having $\chi^2 \leq \chi^2_{\min} + 11.0$, which corresponds to a 90% confidence level region (see Avni 1976; Lampton, Margon, and Bowyer 1976).

We found that β (the gas density distribution) is insensitive to allowed changes in α (the temperature distribution). This is to be expected, since the cooling function is proportional to $T^{-0.6}$ over the temperature range 10^5 to 4×10^7 K (Cowie and McKee 1977), and thus the emissivity varies weakly with temperature. In addition, we required the emission-weighted temperatures corresponding to the values shown in Figure 6 to lie within the 95% confidence range of the measured values.

The results of this procedure constrained α and β such that $0.45 \leq \beta \leq 0.52$ and $-0.4 \leq \alpha \leq 0.6$. With $\alpha = -0.4$ equation (10) becomes

$$M(r) \geq 3.0 \times 10^{11} T_7 r_{10} M_\odot , \quad (11)$$

and thus, for NGC 4472, this more detailed analysis requires a total mass exceeding $2 \times 10^{12} M_\odot$, which is comparable to that obtained by requiring only that the galaxy be sufficiently massive to suppress a wind.

NGC 4472 may not be a typical galaxy. It lies in the Virgo Cluster, and Huchra, Davis, and Latham (1984) have suggested that it is the central member of a separate concentration of galaxies whose mean velocity and line-of-sight velocity dispersion are 1011 and 274 km s^{-1}. Thus, one could argue that the large mass we observe around NGC 4472 has been produced by interactions (tidal stripping, cannibalization) with the other members of its group.

Since spatially resolved temperature measurements are generally not available from present *Einstein* observations for galaxies in this sample, we have estimated total masses of galaxies with measured surface brightness profiles by assuming that the gas is isothermal. This assumption can be justified, since, as argued by Norman and Silk (1979), thermal conduction serves to maintain isothermality in the outer regions of the coronae. Departures due to possible cooling flows in the galaxy core do not significantly affect the estimates of the total mass. The total masses, $M_{\rm tot}$, in Table 2 range from $\sim$(1–5) $\times 10^{12} M_\odot$ and are computed to the maximum galaxy radius for which X-ray emission is detected.

c) *Comparison of Mass-to-Light Ratios of Early-Type Galaxies, Spiral Galaxies, Groups, and Clusters*

The scarcity in early-type galaxies of tracers used to study the dynamics of spirals has prevented the determination of their total masses (at large radii) and mass-to-light ratios. The X-ray coronae, as has been shown above, can be used to compute the total gravitational mass, extending beyond the Holmberg radius of the galaxy. Using the masses derived in § III*b* and the blue luminosities from Table 1, we have derived mass-to-light ratios (in solar units) for the galaxies with measured X-ray surface brightness profiles (Table 2). The values of $M_{\rm tot}/L_B$ are computed from the total mass within the radius, $R_{\rm max}$, to which the X-ray emission is detected (Table 2, col. [4]). The observed extent depends on the galaxy's X-ray luminosity and the effective exposure time (sensitivity) of the X-ray observation. Therefore, the mass-to-light ratios given in Table 2 are appropriate for that radius and should be considered lower limits to the total galaxy mass-to-light ratio. Because of limitations in detecting faint X-ray surface brightnesses, our analysis may not have determined the entire underlying galaxy

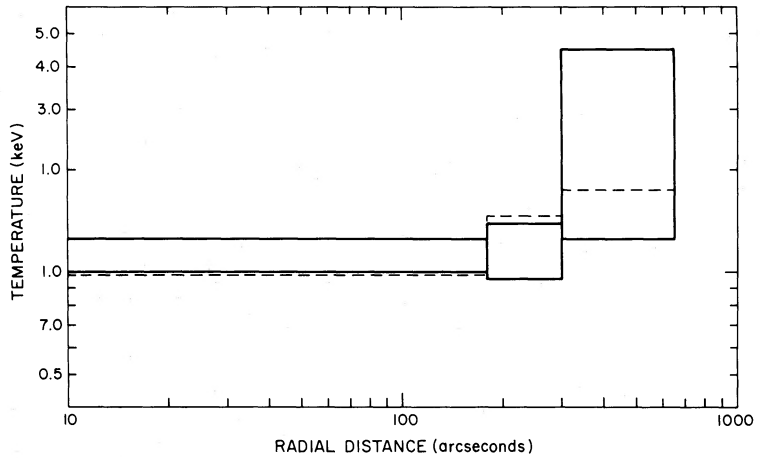

FIG. 6.—The best fit temperatures to the observed pulse-height data of NGC 4472 divided into three radial regions are shown as solid lines which delineate the 90% confidence region for each radial bin. Also shown are the emission-weighted temperatures (*dashed lines*) derived from a model which reproduces the observed surface brightness distribution and has the steepest temperature gradient consistent with our observations.

mass. Therefore differences in M_{tot}/L_B from one galaxy to another may not be significant, since a longer X-ray exposure could result in a larger R_{max} and hence a larger M_{tot}.

The resulting values of M_{tot}/L_B for the early-type galaxies range up to ~ 100. These high values imply that much of the matter around these galaxies is not in luminous form, since the stellar matter has values of $M_{stellar}/L_B$ of only 5–10 (Faber and Gallagher 1979). The X-ray observations of hot coronae around early-type galaxies and the flat rotation curves found for spiral galaxies argue that galaxies of all Hubble types possess dark halos.

Blumenthal *et al.* (1984, hereafter BFPR) have summarized the mass-to-light ratios of a variety of systems ranging from individual galaxies to large clusters. For elliptical-dominated groups BFPR give a mass-to-light ratio of 73–163, overlapping the range we observe for individual galaxies. Therefore, the dark matter in elliptical-rich groups may well be of the same type as that observed around E and S0 galaxies.

BFPR have computed the ratio of total to luminous (in any wavelength region) matter, M_{tot}/M_{Lum}, and have found that this ratio is apparently constant on different mass scales. For clusters, this ratio is $8.4\,(+7.0, -1.0)$, while our sample of elliptical galaxies gives values up to ~ 15 ($M/L_B = 6$ for the stellar matter). If early-type galaxies expel amounts of gas per unit luminosity comparable to those expelled by galaxies in clusters (see § III*d*), and if this ejected mass is taken into account in the calculation of M_{tot}/M_{Lum} for galaxies in our sample, then M_{tot}/M_{Lum} is at most ~ 5. These values of M_{tot}/M_{Lum} for individual galaxies are very uncertain because they depend on the fraction of heavy elements produced by the first generations of stars, which governs the portion of the intracluster medium (ICM) that is attributed to mass loss from galaxies. As the values of M_{tot}/M_{Lum} suggest, individual early-type galaxies may have amounts of dark matter per unit luminous matter comparable to the amounts in clusters and groups. This suggests that much of the dark matter in clusters may once have been part of the constituent galaxies and, in particular, formed their halos. This conclusion is supported by our observation of X-ray coronae, and therefore dark halos, around galaxies in the Virgo Cluster, as well as around galaxies in small groups.

d) The Origin and Fate of Gas in Early-Type Galaxies

We have used X-ray observations to determine the present mass in diffuse hot gas around early-type galaxies. These masses (Table 2) are effectively lower limits, since somewhat more matter could be stored at larger radii (beyond R_{max}) where our sensitivity is insufficient to detect its low surface brightness emission. The gas masses we observe are equal within the uncertainties to those predicted by the accumulation of gas lost by present generation stellar systems (see Fig. 5 and eq. [3]). However, much larger amounts of gas are predicted to be lost by young stellar systems at early stages of galaxy evolution. The integrated mass loss from birth to the present would yield a time-averaged mass loss rate 50 times higher than the present epoch value (FG; MB). The bulk of this matter would be produced in a short interval of time (along with an above average amount of energy from the deaths of massive first generations of stars; see, e.g., De Young 1978). Thus, either the gas observed in galactic coronae may be mass accumulated using present epoch mass loss rates, or, if the true values of present epoch mass loss are near their lowest allowed values (FG cite an uncertainty of a factor of 3), most of the X-ray–emitting gas would be that remaining (not ejected or recycled) from the earliest stages of galaxy evolution. If, for example, galaxies retained a mass of gas proportional to their stellar masses, then the dependence of L_x on L_B (in eq. [3]) is still explainable.

We can estimate the total mass of gas lost to the intergalactic medium by galaxies like those in our sample by comparing them with galaxies in rich clusters. The half-solar abundance of iron in the ICM (e.g., Mushotzky 1984) suggests that a large fraction of the ICM gas was processed through the constituent galaxies. Using models of nucleosynthesis, De Young (1978) argued that roughly 50% of the ICM could be primordial. BFPR note that $M_{tot}/L_B \sim 300$ for rich clusters and that the gas mass is $\sim 10\%$ of the virial mass. Therefore, $M_{gas}/L_B \sim 30$ for rich clusters. M_{gas}/L_B could be reduced if substantial amounts of light are in faint galaxies or diffuse light. For our galaxy sample, we find that $M_{gas}/L_B \leq 0.4$ (gas mass from Table 2 and M_B from Table 1) and that the average value of this ratio is 0.16 for all galaxies in Table 2. Larger values could result if the coronae extend to fainter surface brightness levels than we can detect. Nonetheless, per unit luminosity, rich clusters (e.g., Coma) contain much more matter in gaseous forms that do individual galaxies in less dense environments. If we are not to attribute large differences to early-type galaxies in rich clusters compared with those in less dense environments, then all early-type galaxies must have liberated large amounts of enriched material. We take the difference between the gas mass per unit luminosity in early-type galaxies and assume that half the intracluster medium is gas lost from galaxies, to estimate how much mass the early-type field galaxies must have expelled into the intergalactic medium (IGM). This value is $\sim 15\ M_\odot$ of gas per unit solar luminosity. Then, using the luminosity density of galaxies of $6 \times 10^{-11}\ L_\odot\ \mathrm{pc}^{-3}$ (Davis, Geller, and Huchra 1978) and assuming that 20% of field galaxies are early type, we compute an IGM density of $7 \times 10^{-9}\ \mathrm{cm}^{-3}$. Although this density is quite uncertain because of the factors noted above, early-type galaxies can be substantial contributors to the IGM.

IV. CONCLUSIONS

The observations of extended X-ray emission around early-type galaxies have led to the following conclusions:

1. Optically luminous ($M_B < -19$) early-type galaxies are generally surrounded by envelopes of hot gas ($T \sim 10^7$ K).

2. The gas comprising galactic coronae can be understood as the material accumulated by the galaxy over its lifetime from the normal evolution of its stellar component. Early-type galaxies do not presently drive hot galactic winds.

3. The X-ray luminosity for early-type galaxies (having no substantial cool interstellar medium component) is roughly proportional to the square of their optical (blue) luminosity. This is consistent with models of hot gaseous coronae if they all have comparable structure.

4. While the gas is only a small fraction of the galaxy mass, it can serve as an ideal probe of the mass distribution in the outer regions of early-type galaxies. For isothermal coronae, our observations suggest that early-type galaxies, as a class, have massive dark halos with mass-to-light ratios as large as 100 (in solar units). Thus the X-ray observations of early systems complement the radio and optical observations which have been powerful probes for investigating the outer regions of spiral galaxies.

5. The mass-to-light ratios derived for early-type galaxies are consistent with those of elliptical-dominated groups and

approach those of rich clusters (although in these systems the dark matter is probably no longer associated with the individual galaxies). The similarity of mass-to-light ratios between early-type galaxies and the larger group and cluster structures suggests that much of the dark matter in the larger dynamical systems could once have been associated with their constituent galaxies.

6. The ratio of total mass to luminous mass, $M_{\rm tot}/M_{\rm Lum}$, was found by Blumenthal *et al.* (1984) to be $\sim$5–15 for a range of dynamical systems including dwarf galaxies, elliptical and spiral groups, and large clusters. The missing datum, the total mass of individual early-type galaxies, has now been determined through the analysis of the X-ray coronae and yields similar values.

7. A comparison of the gas mass per unit luminosity in early-type galaxies and rich clusters suggests that early-type galaxies in the field have lost most of the gas they produced at early epochs. This gas would produce an IGM with density $\sim 7 \times 10^{-9}\,{\rm cm}^{-3}$.

The discovery of hot coronae as a common feature of early-type galaxies opens up a new avenue of study for X-ray astronomy and a new way of investigating early-type galaxies. Among the rich variety of problems which are addressable through the X-ray observations are the possible cooling flows which may occur in the cores of these systems. In addition to the type of analyses presented above, one also should be able to investigate the elemental abundance of the coronal gas (as a function of radial distance from the galaxy) because of the strong line emission from 10^7 K gas. Thus, one can study the heavy-element enrichment and its history. These results will have fundamental implications for understanding the metal enrichment and the amount of primordial gas in the ICM of clusters of galaxies.

We thank M. DeFaccio and C. Stern for help with the data analysis. We would like to thank H. Tananbaum and L. Van Speybroeck for their careful reading of this paper. We thank D. Fabricant for his help in using the most recent calibration of the IPC in our spectral analysis. We also thank I. Gioia, D. Harris, and R. Rosner for their helpful comments. J. Bregman patiently discussed the physics of galactic winds with us and communicated to us his calculations of the conditions for the onset of winds. We thank A. Fabian for allowing us to include his NGC 1395 observations. K. Modestino expertly prepared the manuscript.

This work was supported by NASA contract NAS8-30751.

REFERENCES

Avni, Y. 1976, *Ap. J.*, **210**, 642.
Bechtold, J., Forman, W., Giacconi, R., Jones, C., Schwarz, J., Tucker, W., and Van Speybroeck, L. 1983, *Ap. J.*, **265**, 26.
Biermann, P., and Kronberg, P. 1983, *Ap. J. (Letters)*, **268**, L69.
Blumenthal, G., Faber, S., Primack, J., and Rees, M. 1984, preprint.
Bregman, J. 1984, private communication.
Burstein, D., Rubin, V., Thonnard, N., and Ford, W. K. 1982, *Ap. J.*, **253**, 70.
Caldwell, N. 1982, Ph.D. thesis, Yale University.
———. 1984, *Ap. J.*, **278**, 96.
Carter, D., Inglis, I., Ellis, R., Efstathiou, G., and Godwin, J. 1984, preprint.
Cowie, L., and McKee, C. 1977, *Ap. J.*, **211**, 135.
Daltabuit, E., and Meyer, S. 1972, *Astr. Ap.*, **20**, 415.
Davies, R., Efstathiou, G., Fall, S. M., Illingworth, G., and Schechter, P. 1983, *Ap. J.*, **266**, 41.
Davies, R., and Illingworth, G. 1983, *Ap. J.*, **266**, 516.
Davis, M., Geller, M., and Huchra, J. 1978, *Ap. J.*, **221**, 1.
de Vaucouleurs, G. 1975, in *Stars and Stellar Systems*, Vol. **9**, *Galaxies and the Universe*, ed. A. Sandage, M. Sandage, and J. Kristian (Chicago: University of Chicago Press), p. 557.
de Vaucouleurs, G., and de Vaucouleurs, A. and Corwin, H. 1976, *Second Reference Catalogue of Bright Galaxies* (Austin: University of Texas Press).
De Young, D. S. 1978, *Ap. J.*, **223**, 47.
Dressler, A. 1979, *Ap. J.*, **231**, 659.
Dressler, A. 1984, *Ap. J.*, **281**, 512.
Dressler, A., and Sandage, A. 1983, *Ap. J.*, **265**, 664.
Fabbiano, G., Trinchieri, G., and Macdonald, A. 1984, *Ap. J.*, **284**, 65.
Faber, S. M., and Gallagher, J. S. 1976, *Ap. J.*, **204**, 365 (FG).
———. 1979, *Ann Rev. Astr. Ap.*, **17**, 135.
Fabian, A. C., and Khembavi, A. K. 1982, in *IAU Symposium 97, Extragalactic Radio Sources*, ed. D. Heeschen and C. Wade (Dordrecht: Reidel), p. 453.
Fabian, A. C., Schwarz, J., and Forman, W. 1980, *M.N.R.A.S.*, **192**, 135.
Fabricant, D., and Gorenstein, P. 1983, *Ap. J.*, **267**, 535.
Feigelson, E. D., Schreier, E. J., Delvaille, J. P., Giacconi, R., Grindlay, J. E., and Lightman, A. P. 1981, *Ap. J.*, **251**, 31.
Forman, W., Schwarz, J., Jones, C., Liller, W., and Fabian, A. 1979, *Ap. J. (Letters)*, **234**, L27.
Geller, M. J. and Huchra, J. P. 1983, *Ap. J. Suppl.*, **52**, 61.
Gould, R. 1980, *Ap. J.*, **238**, 1026.
Harris, W., and Racine, R. 1979, *Ann. Rev. Astr. Ap.*, **17**, 241.
Heiles, C. 1975, *Astr. Ap. Suppl.*, **20**, 37.
Hertz, P., and Grindlay, J. 1983, *Ap. J.*, **275**, 105.
Huchra, J. P. 1984, private communication.
Huchra, J. P., Davis, R., and Latham, D. 1984, in *Proc. Trieste Meeting on Clusters and Groups of Galaxies*, ed. F. Mardirossian, in press.
Huchra, J. P., and Geller, M. J. 1982, *Ap. J.*, **257**, 423.
Illingworth, G. 1977, *Ap. J. (Letters)*, **218**, L43.
Jones, C. 1977, *Ap. J.*, **214**, 856.
Kormendy, J., and Illingworth, G. 1982, *Ap. J.*, **256**, 460.
Lampton, M., Margon, B., and Bowyer, S. 1976, *Ap. J.*, **208**, 177.
Long, K., and Van Speybroeck, L. 1983, in *Accretion-driven Stellar X-Ray Sources*, ed. W. Lewin and E. van den Heuvel (Cambridge: Cambridge University Press), p. 117.
Mathews, W., and Baker, J. 1971, *Ap. J.*, **170**, 241 (MB).
McKee, C., and Cowie, L. 1977, *Ap. J.*, **215**, 213.
McKee, C., and Ostriker, J. 1977, *Ap. J.*, **218**, 148.
Mushotzky, R. F. 1984, *Phys. Scripta*, **T7**, 157.
Norman, C., and Silk, J. 1979, *Ap. J. (Letters)*, **233**, L1.
Nulsen, P., Stewart, G., and Fabian, A. 1984, *M.N.R.A.S.*, **208**, 185.
Raymond, J., Cox, D., and Smith, B. 1976, *Ap. J.*, **204**, 290.
Rosner, R. 1984, private communication.
Rubin, V., Burstein, D., and Thonnard, N. 1980, *Ap. J. (Letters)*, **242**, L149.
Rubin, V., Ford, W. K., and Thonnard, N. 1978, *Ap. J. (Letters)*, **225**, L107.
———. 1980, *Ap. J.*, **238**, 471.
Rubin, V., Ford, W. K., Thonnard, N., and Burstein, D. 1982, *Ap. J.*, **261**, 439.
Sandage, A., and Tammann, G. A. 1981, *A Revised Shapley-Ames Catalog of Bright Galaxies* (Austin: University of Texas Press).
Sandage, A., and Visvanathan, N. 1978, *Ap. J.*, **223**, 707.
Sanders, R. 1981, *Ap. J.*, **244**, 820.
Schreier, E. J., Feigelson, E., Delvaille, J., Giacconi, R., Grindlay, J., Schwartz, D. A., and Fabian, A. C. 1979, *Ap. J. (Letters)*, **234**, L39.
Spinrad, H., and Taylor, B. J. 1971, *Ap. J., Suppl.*, **22**, 445.
Stanger, V., and Schwarz, J. 1984, preprint.
Tammann, G. A. 1982, in *Supernovae: A Survey of Current Research*, ed. M. Rees and R. Stoneham (Dordrecht: Reidel).
Thuan, T., and Romanishin, W. 1981, *Ap. J.*, **248**, 439.
Tonry, J. 1982, *Ap. J. (Letters)*, **251**, L1.
Trinchieri, G., and Fabbiano, G. 1984, *Ap. J.*, submitted.
Van Speybroeck, L. 1984, private communication.
White, R., and Chevalier, R. 1984, *Ap. J.*, **280**, 561.

W. Forman and C. Jones: Harvard-Smithsonian Center for Astrophysics, 60 Garden Street, Cambridge, MA 02138

W. Tucker: P.O. Box 266, Bonsall, CA 92003